8

Contact Angle Measurements on Fibers and Fiber Assemblies, Bundles, Fabrics, and Textiles

BIHAI SONG Krüss GmbH, Hamburg, Germany

ALEXANDER BISMARCK Imperial College London, London, United Kingdom

JÜRGEN SPRINGER Technical University of Berlin, Berlin, Germany

I. INTRODUCTION

The study of fiber wettability has important implications in detergency [1], water and oil repellency of textiles [2], in textile spinning, optical fiber processing, and in the chemical design of modern fiber reinforced composite systems (such as fiber reinforced polymers or concrete). The degree to which a liquid wets fibers determines how easily the liquid can penetrate fiber assemblages and this is important for both wet processing and for the performance of a textile article. Understanding the nature of the interaction of fibers with various liquids is important to tailor new polymeric composite systems [3]. The measurement of contact angles provides useful information about their wettability. The latter is essential in the modification of the fiber surface state or the adjustment of the rheological properties of the wetting prepolymer (resins) or of a polymer melt. Thermodynamic parameters, such as solid surface tension calculated from measured contact angles and surface polarity, can be used to estimate the expected adhesion between reinforcing fibers and a surrounding matrix [4,5]. It can also lead to a prediction of the compatibility of the components of composite materials.

The wetting behavior of a planar surface is governed by the materials surface chemistry and its local geometry (roughness). The wetting of a fiber of a chemically identical material is, however, significantly different because of the global geometry of the cylindrical shape [6]. The contact angle of a liquid against a fiber is the quantity, which is a fundamental measure [7].

Contact angle measurements provide only information about the outermost atom layers of a surface (~ 0.5 to 1 nm [8]), depending on the chemistry and the molar volume of the liquid used, whereas spectroscopic techniques, such as X-ray photoelectron spectroscopy (XPS) also known as electron spectroscopy for chemical analysis (ESCA), give information about the elemental composition and the bonding state of the elements originating from a cone typically extending some 3–5 nm deep [9]. Therefore contact angle measurements are most suitable for characterizing the changes in the surface "nature" with a high degree of accuracy.

II. CONTACT ANGLES AND WETTABILITY

Wettability refers to the interactions when a liquid l is brought into contact with a solid surface s initially surrounded by a gas (or the saturated liquid vapor v atmosphere) or another liquid [10]. These interactions can result in spreading without limits of the liquid over the surface displacing the other fluid, or the spreading process might come to an end if the equilibrium state is reached, which is characterized by a contact angle θ between the liquid–fluid and liquid–solid interfaces. This phenomenon is often described by a sessile drop resting on a solid surface (Fig. 1).

Young's equation

$$\gamma_{sv} = \gamma_{sl} + \gamma_{lv} \cos \theta \tag{1}$$

connects the quantities of the liquid vapor surface tension γ_{lv}, the solid vapor surface tension γ_{sv}, the solid–liquid interfacial tension γ_{sl}, and the contact angle θ [11]. Young's equation, however, is only applicable to systems that are in equilibrium. This means that all components have a uniform chemical potential in all (liquid, solid, and vapor) phases. Therefore the liquid must be saturated with the solid, which usually lowers the liquid surface tension, and the vapor and solid surface must be at adsorption equilibrium. The value of the interfacial tension of a solid, covered by a film γ_{sv}, is lower than that for the

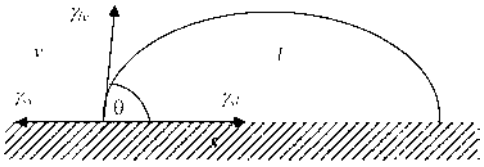

FIG. 1 A drop of liquid l resting on a plane surface of solid s in equilibrium with the liquid's vapor v.

solid-vacuum surface γ_s by the amount of the surface (or spreading or film) pressure π,

$$\pi = \gamma_s - \gamma_{sv}. \tag{2}$$

It is generally accepted that for systems exhibiting contact angles $\theta > 10^\circ$ the surface pressure is negligible [8]. This is usually explained by the fact that a liquid will not adsorb on a solid having a lower surface tension than the liquid [12]. Hence we can write: $\gamma_{sv} \cong \gamma_s$. On the other hand $\gamma_{lv} \cong \gamma_l$, because the interacting energies between the molecules at the surfaces of condensed phases and those in the saturated vapor phase are negligible, compared to the interaction energies acting within the condensed phase [13]. Therefore Young's equation can be written as follows:

$$\gamma_s = \gamma_{sl} + \gamma_l \cos \theta. \tag{3}$$

The only directly measurable quantities in Eq. (3) are the liquid surface tension and the contact angle.

III. DIRECT CONTACT ANGLE MEASUREMENTS FROM THE MENISCUS PROFILES OF DROP-ON-FIBER SYSTEMS

A. Theoretical Background

1. Description of Drop Profile

Like all liquid–fluid interfaces, the equilibrium shape of the interface for a drop-on-fiber system is governed by the gravitational and interfacial tension effects through the classical Laplace equation of capillarity:

$$\Delta p = \gamma \left(\frac{1}{R_1} + \frac{1}{R_2} \right), \tag{4}$$

where Δp is the pressure difference (excess pressure within the drop) across the droplet's liquid–fluid interface, γ is the interfacial tension, and R_1 and R_2 are the principal radii of curvature at a point in the interface.

For a cylinder symmetrical interface as depicted in Fig. 2, R_1 (in the paper plane) and R_2 (perpendicular to the paper plane and to the drop profile $y = f(x)$ depicted in Fig. 2) can be written as

$$\frac{1}{R_1} = \frac{d\phi}{ds} = \frac{d\phi}{dx/\cos \phi} = \frac{d\phi}{dx} \cos \phi, \tag{5}$$

$$\frac{1}{R_2} = \frac{\sin \phi}{x}. \tag{6}$$

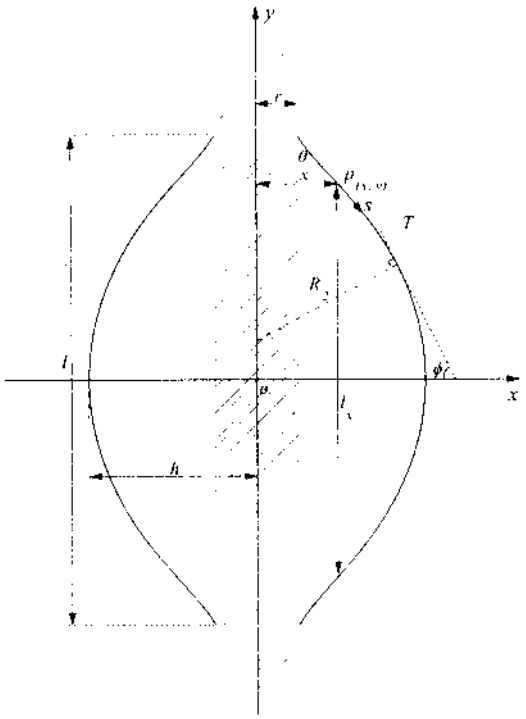

FIG. 2 Geometry and notation of symbols of a drop-on-fiber system.

Eq. (4) may be then rewritten as:

$$\frac{\Delta p}{\gamma} = \cos\phi \frac{d\phi}{dx} + \frac{\sin\phi}{x} = \frac{1}{x}\frac{d}{dx}(x \sin\phi). \tag{7}$$

For very small liquid droplets, the gravitational effect may be negligibly small compared to the interfacial tension, so the term $\Delta p/\gamma$ on the left side of Eq. (7) can be considered constant along the whole interface. Eq. (7) can be then integrated to:

$$x \sin\phi = \frac{1}{2}\frac{\Delta p}{\gamma}x^2 + C_2 = \frac{1}{2}C_1 x^2 + C_2, \tag{8}$$

where C_1 ($= \Delta p/\gamma$) and C_2 are the system constants, which are restricted to the following boundary conditions

$$\begin{aligned} x_{\phi = \pi/2} &= h, \\ x_{\phi = \pi/2 - \theta} &= r. \end{aligned} \tag{9}$$

Combination of Eqs. (8) and (9) gives:

$$x \sin \phi = \left(\frac{h - r \cos \theta}{h^2 - r^2}\right) x^2 + \left(\frac{h \cos \theta - r}{h^2 - r^2}\right) h \cdot r. \tag{10}$$

Eq. (10), together with the relationship:

$$\frac{\mathrm{d}y}{\mathrm{d}x} = -\tan \phi = -\frac{\sin \phi}{\sqrt{1 - \sin^2 \phi}}, \tag{11}$$

allows now the gradient of the drop profile, $\mathrm{d}y/\mathrm{d}x$, to be expressed as a function of x, which, after substitution for $\sin\phi$ in Eq. (11) with the expression of Eq. (10) followed by expansion and simplification as described in detail by Carroll [19], can be written as:

$$-\frac{\mathrm{d}y}{\mathrm{d}x} = \frac{x^2 + a \cdot h \cdot r}{[(h^2 - x^2)(x^2 - a^2 r^2)]^{\frac{1}{2}}}, \tag{12}$$

where a is defined as:

$$a = \frac{h \cdot \cos \theta - r}{h - r \cdot \cos \theta}. \tag{13}$$

With the following transformation:

$$x^2 = h^2 \left(1 - k^2 \sin^2 \varphi\right), \tag{14}$$

where

$$k^2 = \frac{h^2 - a^2 \cdot r^2}{h^2}, \tag{15}$$

Eq. (12) can be rewritten as

$$\mathrm{d}y = \pm \frac{a \cdot r + h(1 - k^2 \sin^2 \varphi)}{(1 - k^2 \sin^2 \varphi)^{\frac{1}{2}}} \mathrm{d}\varphi, \tag{16}$$

which can further be integrated to give

$$y = \pm [a \cdot r \cdot F(\varphi, k) + h \cdot E(\varphi, k)], \tag{17}$$

where $F(\varphi,k)$ and $E(\varphi,k)$ are the Legendre standard incomplete elliptic integrals of the first and second kind, respectively, and are defined as

$$F(\varphi, k) = \int_0^{\varphi} \frac{\mathrm{d}\vartheta}{\sqrt{1 - k^2 \sin^2 \vartheta}}, \tag{18}$$

$$E(\varphi, k) = \int_0^{\varphi} \sqrt{1 - k^2 \sin^2 \vartheta}\, \mathrm{d}\vartheta. \tag{19}$$

Equations (12)–(15) and (17) give the expression of the drop profile in a drop-on-fiber system where the gravitational effect is negligibly small compared to the interfacial tension. To make it easier for the later generalization, it is useful to transfer these equations into their corresponding dimensionless forms by dividing all the used dimensional variables by the radius of the fiber r_f involved in the system:

$$a = \frac{H \cdot \cos\ \theta - 1}{H - \cos\ \theta}, \tag{13a}$$

$$X^2 = H^2(1 - k^2 \sin^2 \varphi), \tag{14a}$$

$$k^2 = 1 - a^2/H^2, \tag{15a}$$

$$Y = \pm[a \cdot F(\varphi, k) + H \cdot E(\varphi, k)], \tag{17a}$$

where X, Y, and H are the dimensionless counterparts of x, y, and h, respectively (in this text we use capital and lowercase letters to describe the dimensionless and dimensional variables, respectively). As can be seen from these relations, a drop profile, as represented by a collection of (X, Y)-coordinates, may be expressed as a function of H and θ and can be obtained through the numeric evaluation of the elliptic integrals F and E in Eq. (14a) and (16a). The Legendre's standard elliptic integrals F and E can be transformed to the Carlson's elliptic integrals [14,15] of the first and the second kind, R_F and R_D, which are more suitable for the numerical evaluation [16,17]:

$$F(\varphi, k) = \sin\ \varphi \cdot R_F(\cos^2\ \varphi, 1 - k^2 \sin^2 \varphi, 1), \tag{20}$$

$$\begin{aligned} E(\varphi, k) = {} & \sin\ \varphi \cdot R_F(\cos^2\ \varphi, 1 - k^2 \sin^2 \varphi, 1) - \frac{1}{3} \cdot k^2 \cdot \sin^3 \varphi \\ & \cdot R_D(\cos^2\ \varphi, 1 - k^2 \sin^2 \varphi, 1). \end{aligned} \tag{21}$$

B. Diverse Characteristic Drop Parameters

(a) Drop Length. Combining Eq. (17a) with Eqs. (20) and (21), one obtains the dimensionless length L of a droplet with maximum height H and contact angle θ:

$$L = 2\left[(a + H) \cdot \sin\ \varphi \cdot R_F - \frac{1}{3} \cdot H \cdot k^2 \cdot \sin^3\ \varphi \cdot R_D\right] = f(H, \theta). \tag{22}$$

The right side in Eq. (22) is a function of H and θ only [as denoted by $f(H,\theta)$], which means that the contact angle θ in a drop-on-fiber system can be unambiguously determined from its length L and height H.

(b) Drop Volume. The (net) liquid volume v of a droplet is calculated from the total volume enclosed under the drop–vapor interface by subtraction of the fiber volume inside the droplet:

$$v = \int_{-\frac{1}{2}}^{\frac{1}{2}} \pi \cdot \left(x^2 - r^2\right) \mathrm{d}y = 2\pi \int_{0}^{\frac{1}{2}} (x^2 - r^2) \mathrm{d}y. \tag{23}$$

Using Eqs. (12) and (14) the above expression can be integrated to give:

$$v = \frac{2\pi h}{3}\left[\left(2a^2r^2 + 3arh + 2h^2\right)E(\varphi,k) - a^2r^2F(\varphi,k) + \frac{r}{h}(h^2 - r^2)^{\frac{1}{2}} (r^2 - a^2r^2)^{\frac{1}{2}}\right] - \pi r^2 l \qquad (\text{with } \sin^2\varphi = (h^2-1)/h^2k^2) \tag{24}$$

Eq. (24) may be transformed to the following dimensionless form:

$$V = \frac{2\pi H}{3}\left[\left(2a^2 + 3aH + 2H^2\right)E(\varphi,k) - a^2F(\varphi,k) + \frac{1}{H}(H^2 - 1)^{\frac{1}{2}} (1 - a^2)^{\frac{1}{2}}\right] - \pi r^2 L \qquad (\text{with } \sin^2\varphi = (H^2-1)/H^2k^2) \tag{24a}$$

(c) Contact Areas. There are two interfacial contact areas involved in the system: solid–liquid a_{sl} and liquid–fluid (usually liquid–gas) a_{lv}. The fiber-liquid contact area can be deduced from the length of the droplet l at once $a_{\mathrm{sl}} = 2\pi rl$. The liquid-fluid contact area can be calculated through surface integration of the drop interface:

$$\begin{aligned} a_{\mathrm{lv}} &= \int_{-\frac{1}{2}}^{\frac{1}{2}} 2\pi \cdot x \mathrm{d}s = 4\pi \int_{0}^{\frac{1}{2}} x \mathrm{d}s = 4\pi \int_{0}^{\frac{1}{2}} x \frac{\mathrm{d}x}{\cos\phi} \\ &= 4\pi \int_{0}^{\frac{1}{2}} x \left[1 + \left(\frac{\mathrm{d}y}{\mathrm{d}x}\right)^2\right]^{\frac{1}{2}} \mathrm{d}x. \end{aligned} \tag{25}$$

Using the relationship of Eq. (12) and the transformation (14), Eq. (25) can be integrated to give:

$$a_{\mathrm{lv}} = 4\pi h(ar + h)E(\varphi,k), \tag{25a}$$

which may be further transformed into the following dimensionless form:

$$A_{\mathrm{lv}} = 4\pi H(a + H)E(\varphi,k), \tag{25b}$$

where φ is given by Eq. (14a) with $X = 1$.

(d) Excess Pressure. The excess pressure in the droplet Δp can be deduced from Eqs. (8) and (10):

$$\frac{\Delta p}{\gamma} = \frac{2(h - r\cos\theta)}{h^2 - r^2}. \tag{26}$$

(e) Inflection Angle. The liquid–fluid interface of a droplet may show an inflection point as it approximates the solid–liquid interface. The inflection point occurs when the gradient of the drop profile, dy/dx, reaches a maximum, i.e., where $d^2y/dx^2 = 0$. By substitution of Eq. (12) into the above formulation and after rearrangement, we have:

$$\frac{d^2y}{dx^2} = 0 \quad \Rightarrow \quad x = \pm\sqrt{ahr} \quad \text{or} \quad X = \pm\sqrt{aH}. \tag{27}$$

Using the relationship of the inflection angle θ_i to the gradient of the drop profile $\tan(90-\theta_i) = dy/dx$, and Eqs. (12) and (27) lead to the following expression of θ_i:

$$\tan\theta_i = \frac{H - a}{2\sqrt{aH}}. \tag{28}$$

The relationship given in (Eq. (27) must be, however, restricted to the fact that in a real droplet-on-fiber system the value of X can never be smaller than 1, which leads to:

$$X^2 = aH \geq 1 \quad \Rightarrow \quad \frac{2H}{H^2 + 1} \leq \cos\theta \leq 1 \quad \text{or} \quad H \geq \frac{1 + \sin\theta}{\cos\theta}. \tag{29}$$

Eqs. (29) and (27) indicate that the existence of an inflection point and its location for a given system with a certain contact angle θ is dependent of the droplet size H. It is in general to be observed by droplets with a small contact angle (e.g., $< 30°$), whereas for droplets of small size and large contact angles it may be missed.

It can be verified that for a droplet having a reduced drop height of H, its maximum possible inflection angle α_{max} is equal to its maximum possible contact angle under the fulfillment of Eq. (29) and its minimum possible inflection angle α_{min} occurs at $\theta = 0$:

$$\alpha_{max} = \arcsin\left(\frac{H^2 - 1}{H^2 + 1}\right) \tag{30}$$

$$\alpha_{min} = \arctan\left(\frac{H - 1}{2\sqrt{H}}\right) \tag{31}$$

C. Maximum Drop Length (L)–Height (H) Method

As pointed out above, the right side of Eq. (22) is a function of H and θ only, which suggests that the contact angle θ can be unambiguously determined from the maximum drop length L and height H. Based on this principle, Yamaki and Katayama [18] and Carroll [19] have introduced this method for determining the contact angle of a liquid droplet on a cylindrical fiber surface.

However, Eq. (22) cannot be transformed into an explicit form of contact angle in dependence of H and L. To evaluate the contact angle from the measured H and L, Eq. (22) must be solved numerically in an iterative way. The resolutions are available both in graphical [18,19] and table forms (see table in Appendix A). Because of the complexity of the dependence (see curve a in Fig. 3 [20]), the graphical relationship allows the contact angle generally to be found to within about 5° [16], while the tables provided by Carroll [19] later giving L as a function of H and θ in steps of 0.01 in H and of 1° in θ do make a highly precise determination possible.

To make the determination more accurate than using the graphical relationship and more convenient than using the tables, a computer program

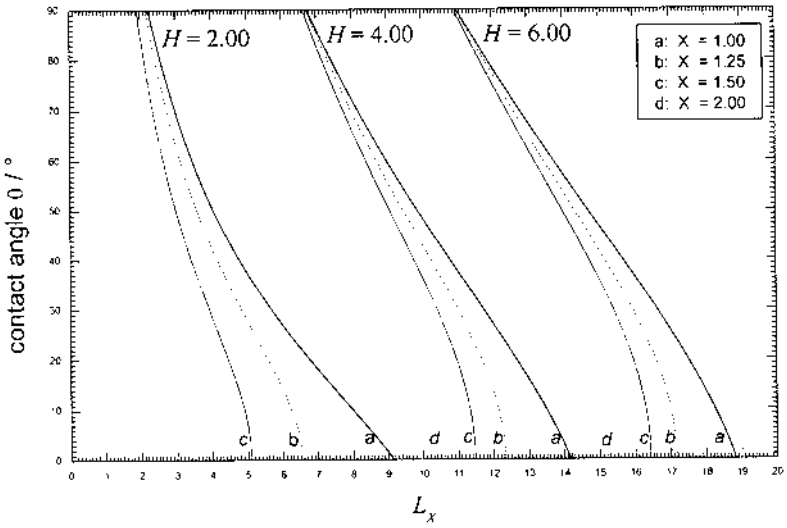

FIG. 3 Contact angle as a function of droplet length at a given height.

may be used to solve Eq. (22) numerically [16]. There are many ways to do it. One of them is by minimizing the following objective function E_{LH}

$$E_{LH} = \left| L - 2\left[(a+H)\cdot \sin\varphi \cdot R_{\mathrm{F}} - \frac{1}{3}\cdot H\cdot k^2 \cdot \sin^3 \cdot R_{\mathrm{D}} \right] \right| = |L - f(H,\theta)| \tag{32}$$

at $X = 1$.

E_{LH} is by given L and H, a one-dimensional function of θ. Any one-dimensional minimization routine may be therefore suitable for solving this problem. For example, the Brent's method in one-dimension as described in Ref. 17 was found to be quite suitable for this purpose [20].

D. Methods Based on the Drop's Inflection Angle

Like the maximum droplet height (H) and length (L), the inflection angle (α) of a droplet is a characteristic parameter, which can be used in combination with other parameters to determine the contact angle. For drops exhibiting a visible (or measurable) inflection angle, the direct measurement of inflection angle may be easier and more accurately practicable than the contact angle itself.

As pointed out above, not all droplets exhibit an inflection angle that must be located within the range of $1 \le X \le H$. For the occurrence of an inflection angle the condition of Eq. (29) must be fulfilled.

Fig. 4 displays the relationship of $\alpha_{\max}$ and $\alpha_{\min}$ in dependence of H. For droplets with a reduced drop height of H, an inflection angle can only be observed if its contact angle lies under the $\alpha_{\max}$ curve, which also determines the applicability of the methods based on inflection angle. For systems with larger contact angles it may be necessary to increase the droplet volume to a certain size, so that an inflection angle can be observed. The applicability of these methods is, in general, restricted for contact angle under 60°.

E. Method Based on Droplet Height and Inflection Angle (H, α Method)

Among the droplet characteristic parameters H, L, α, the maximum reduced droplet height H can be in general determined easily and accurately. Therefore for droplets with inflection angle, if this angle can be measured with appropriate accuracy (e.g., with the help of imaging processes [3]), the combination of H and α will be a very useful alternative for determining the contact angle.

Fig. 5 shows the relationship between the contact angle θ and inflection angle α of a droplet at a given H. It can be seen that the contact angle is very

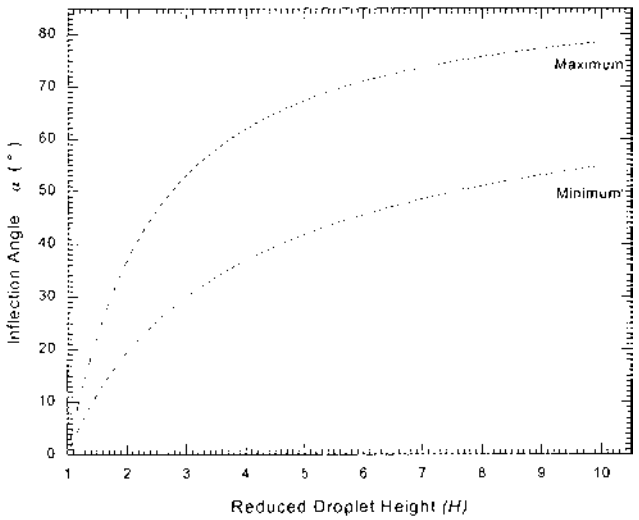

FIG. 4 Dependence of minimal and maximal inflection angle α on H.

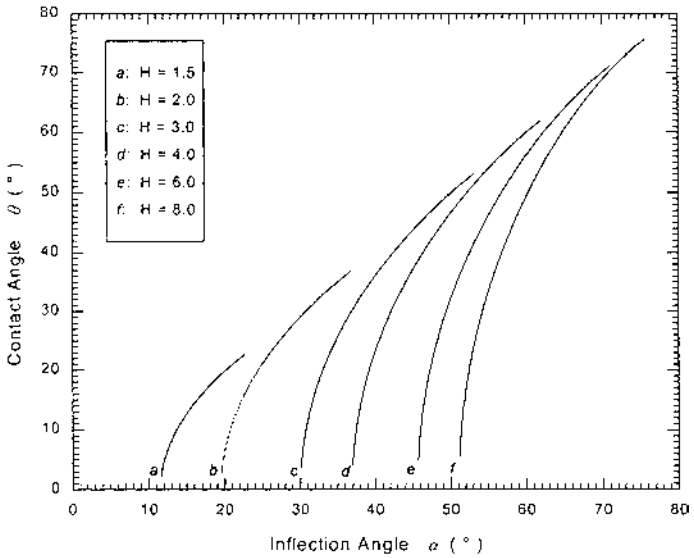

FIG. 5 Dependence of the contact angle θ on inflection angle α at a given H.

sensitive to the variation of the inflection angle, which is especially pronounced in the range of small contact angles ($\theta < 10^\circ$ for small droplets and $\theta < 20^\circ$ for large droplets). An error of 1° in determining the inflection angle can cause an error of about 10° in the resulting contact angle.

This sensitivity subsides as the inflection angle approaches its maximum value at each given H. Nevertheless, at the same time the inflection position moves closer to the three-phase contact (TPC) line and coincides with the TPC point as the inflection angle reaches its maximum, which makes the determination of the inflection angle as difficult as the contact angle itself.

Fig. 6 shows the dependence of the contact angle on H at given inflection angles α. For small contact angles, the relationship is very sensitive; a small uncertainty in the determination of H may cause a large error in the resulting contact angle.

Fig. 7 displays the variation of the inflection angle and its location by changing the droplet size (implied by H) for a given system (i.e., with a given contact angle). The inflection angle increases with increasing droplet volume. At the same time the location of the inflection point moves absolutely away from, but relatively closer to, the solid surface, because the reduced maximum droplet height increases far more rapidly than the movement of the location of the inflection point.

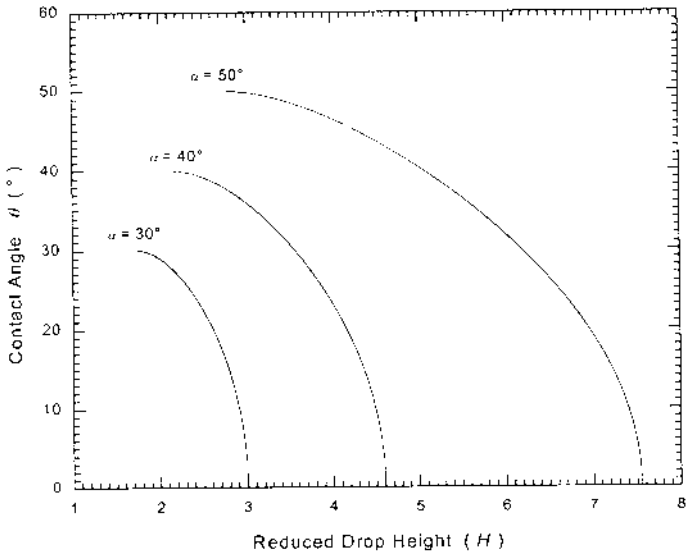

FIG. 6 Contact angle θ as a function of the drop height H for inflection angles α.

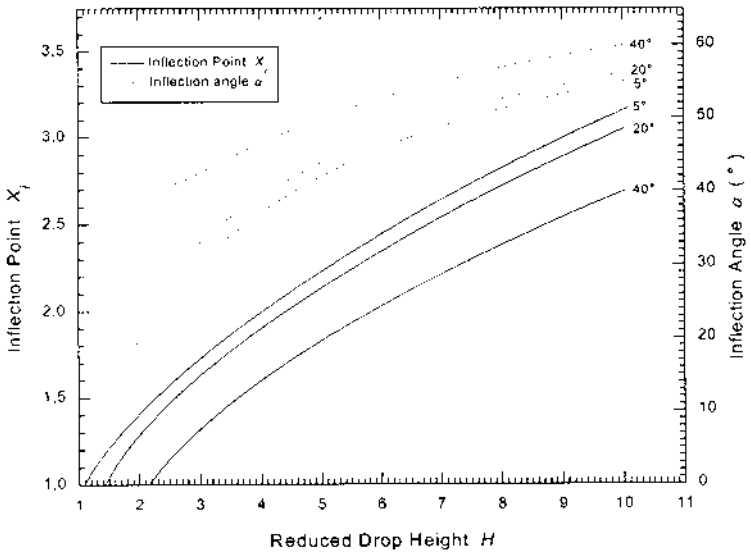

FIG. 7 Inflection angle α and inflection point X_i as a function of the drop size (as indicated by droplet height H) for given contact angles θ.

As a result, the method based on the measurement of H and α is, in general, too error-sensitive to have a wide applicability. Nevertheless, the method can be quite interesting when the inflection angle can be determined with high accuracy, for example, using some appropriate profile analysis routines [2].

F. Method Based on Droplet Length and Inflection Angle (L, α Method)

Similar to the method based on droplet height and inflection angle (H,α method), the contact angle may be determined by measuring the droplet length L and the inflection angle (L,α method). Fig. 8 shows the dependence of the contact angle on the inflection angle by some given drop lengths.

It can be seen from Fig. 8 that the contact angle is not so sensitive to the variation of inflection angle as in case of the H,α method, whereas the value of drop length L is, in general, more difficult to measure precisely than H.

Fig. 9 shows the dependence of the contact angle on L by given inflection angles. For small droplets of small contact angles, the value of the contact

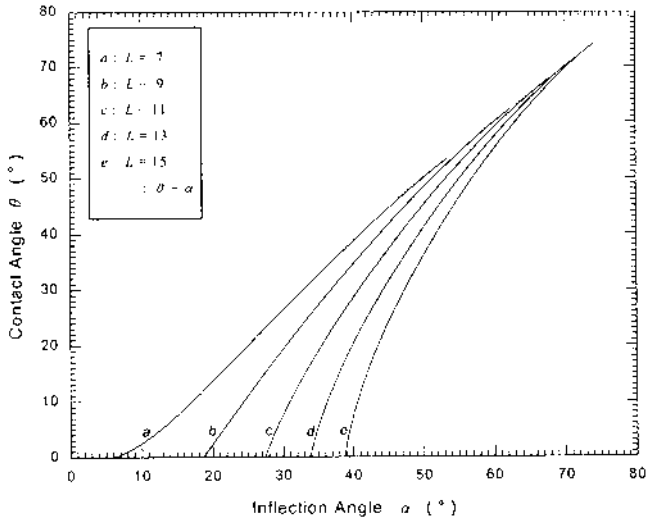

FIG. 8 Dependence of the contact angle θ on the inflection angle α at given drop lengths L.

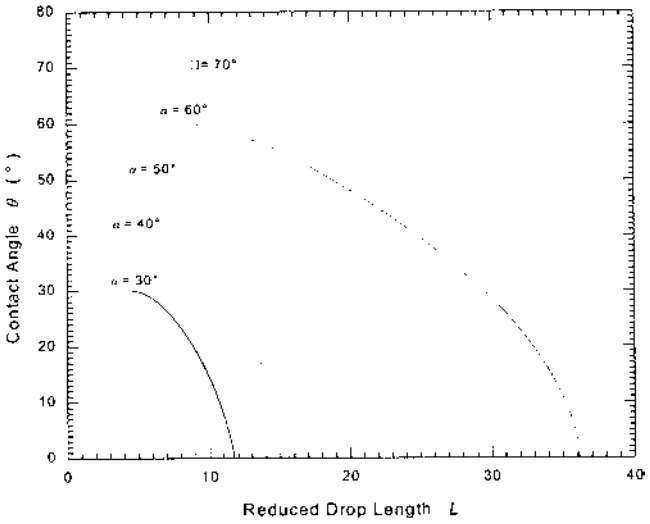

FIG. 9 Dependence of the contact angle θ on the drop length L for given inflection angles α.

angle is much more sensitive to possible uncertainties in the determination of L than for larger droplets with large contact angles.

G. Method Based on Droplet Length, Height, and Inflection Angle (L/H, α Method)

One more imaginable method based on the measurement of the inflection angle is to combine all three droplet characteristic parameters H, L, and α for determining the contact angle. Fig. 10a–c shows the relationship of the inflection angle in dependence of L/H-ratio by given contact angles in steps of 2°. Using L/H-ratio instead of absolute values of L or H replaces the need to determine the fiber radius r_f. This is particularly advantageous because of the fact that the equations have to be transferred into their corresponding dimensionless forms by dividing all the used dimensional variables involved in the system by r_f having a limited accuracy.

H. A Generalized Drop Length (L_x)–Height (H) Method

The maximum L,H method works accurately, insofar as the L- and H-values can be determined with sufficient precision. This is often not the case, however, because the curve of a liquid drop surface changes steeply near the three-phase contact line [18] and the determination of the drop dimensions (especially the L-values) is often associated with large uncertainty and subject to subjective influences. This is particularly true for drops of small contact angles and for cases where the drop dimensions are measured with video images instead of photographs [21]. For fibers of very small diameter (in the order of 1 μm), the formation of "precursor manchon" [22] or "protruding foot" [23] may further complicate the determination of the contact points. Because the value of the contact angle is quite sensitive to the values of L and H, a small uncertainty in the determination of contact points may introduce large errors in the resultant contact angle values and make the determination of contact angles in some cases more or less subjective.

To partially overcome the disadvantages of the maximum L,H method, Song et al. [20] have recently extended the concept and introduced a generalized drop length–height method. Instead of using only the maximum drop length L, together with the maximum drop height H, for calculating the contact angle, a general drop length L_x was introduced. This is the length (i.e., diameter) of a drop measured at the drop plane $X = X$ (see the dimensional representation in Fig. 2). According to this definition we have $L = L_1$, i.e., the maximum drop length is the drop length measured at $X = 1$. As can be seen from Eqs. (14a) and (17a), any combination of L_x and H of a drop profile can

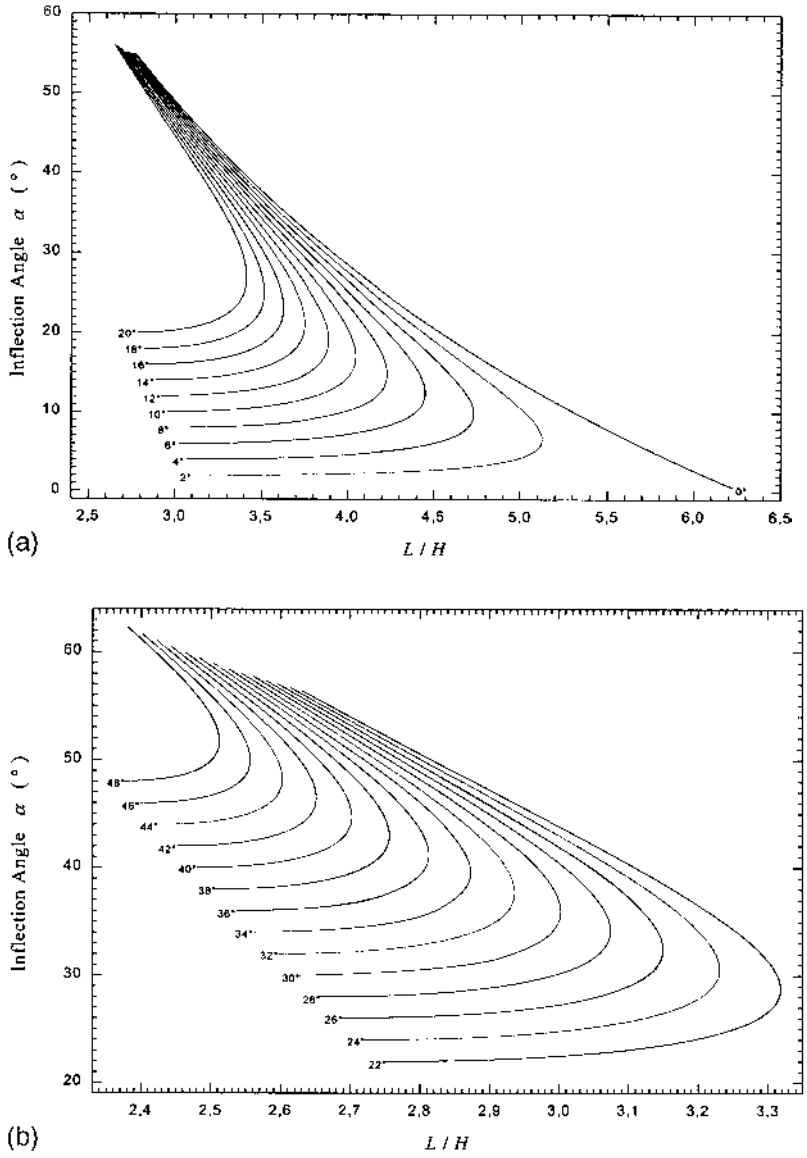

FIG. 10 Inflection angle α as a function of the L/H ratio for given contact angles θ.

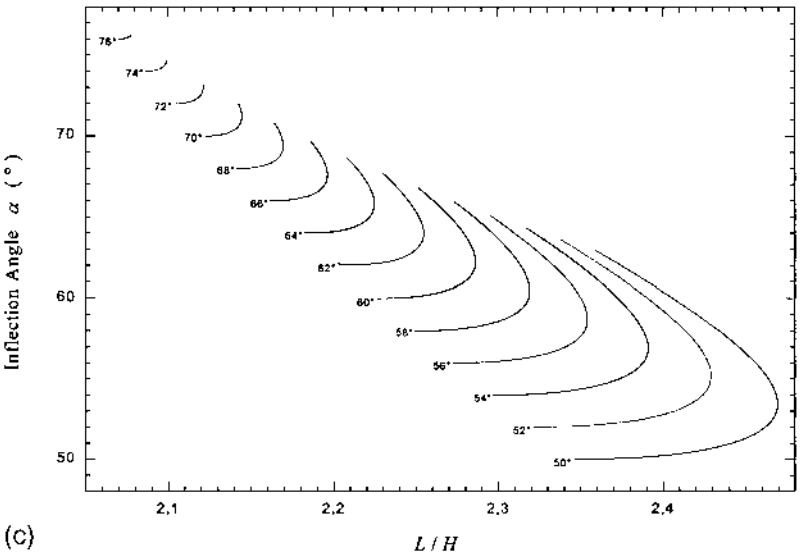

FIG. 10 Continued.

now be used to calculate the contact angle θ. Similarly to the maximum L,H method θ is now determined by minimizing the following objective function $E_{L_x,H}$:

$$E_{L_x,H} = \left| L_x - 2\left[(a+H)\cdot \sin\varphi \cdot R_F - \frac{1}{3}\cdot H \cdot k^2 \cdot \sin^3 \cdot R_D\right]\right| = |L_x - f(H,\theta)| \tag{33}$$

at $X = X$.

Fig. 3 shows, the calculated relationship of contact angles to L_x-values for given drop heights $H = 2$, 4, and 6. The value of the contact angle is increasingly sensitive to the value of L_x with increasing X, particularly for contact angles smaller than 10°. This means that with the same extent of error in L_x-values the error in the resultant contact angle value increases with increasing X. Therefore this new procedure will only work well if the L_x-values at $X > 1.0$ can be determined more accurately than the maximum drop length itself.

One advantage of this generalized method over the common maximum L,H method lies in the fact that one is no more restricted to measuring the maximum drop length in order to determine the contact angle. Alternatively, it is possible to measure the drop length at any drop levels and use the

measured values to calculate the contact angle. As pointed out above, the determination of the maximum drop length is generally associated with uncertainty and subjective influences, because the three-phase contact points are often smeared out and may not be determined with sufficient precision. However, the drop lengths at higher X-levels (e.g., $X > 1.5$) are well defined and may be measured more accurately, which may compensate or overwhelm the weakness of sensitivity by using L_x,H-values with $X > 1$ for computing the contact angle. Compared to the L-value, the maximum drop height H can be, in general, measured with more satisfactory accuracy.

Furthermore, this generalized method provides us with a procedure to determine the contact angle from a number of pairs of L_x,H-values around a drop profile, so that their resultant average value can be more reliable than the value obtained only from the single pair of L,H-values as usually done in the literature. In this way a large part of the whole drop profile can be involved in the determination process, which will reduce the random statistical error and thus improve the accuracy of the measurement.

Principally L_x,H-values at any X-levels can be used to determine the contact angles. However, with increasing X-value, L_x-value decreases, and thus the relative error in its determination rises. The meaningful X-values therefore usually range from 1 to about $H-2$ (for drops with $H > 3$) [20].

1. Theoretical Simulations

Theoretical simulations have been carried out in order to examine the applicability and reliability of the generalized drop length–height L_y,H method as described above. Dimensionless theoretical drop profiles are generated by numerically solving the following equations:

$$X^2 = H^2(1 - k^2 \sin^2 \varphi), \tag{14a}$$

$$Y = \pm[a \cdot F(\varphi, k) + H \cdot E(\varphi, k)]. \tag{17a}$$

The theoretical profiles (i.e., X-coordinates of the profiles) are then overlapped with random errors in order to simulate the experimentally obtained drop profiles. As a typical example we have shown in Fig. 11 a simulated drop profile with $H = 3$ and $\theta = 15°$.

Contact angles were then evaluated from the profiles using the program described in Ref. 20. The result of applying the L_y,H method to the profile shown in Fig. 11 is plotted in Fig. 12.

Generated profiles were not the same, as they were all overlaid with random errors and, therefore, the calculation for every H–θ combination included in the table was repeated 40 times. Table 1 contains some of the results, the average values, and the standard deviation for each H–θ-combination. The maximum extent of the overlaid random error amounts to 0.025, which is

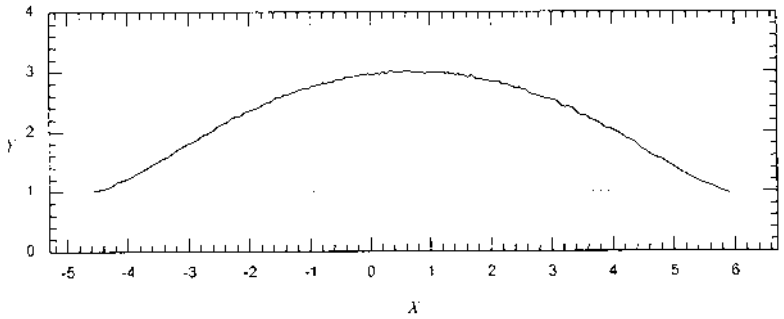

FIG. 11 A simulated (dimensionless) drop profile overlapped with random errors with a maximum content of 0.025.

close to the maximum statistical errors of real drop profiles extracted using digital image processing.

2. Experimental Measurements

The L_x,H method was successfully applied to study a variety of drop-on-fiber systems [20,24] and also to characterize the wetting behavior of (carbon) fiber–polymer melt systems [25–27]. Fig. 13 shows exemplarily a drop of polyimide (Pl, Aurum PD 400) melt on a carbon fiber (Toray T700SC) at 420°C in air atmosphere together with the extracted drop profile. The carbon fibers studied have diameters of approx. 7 μm.

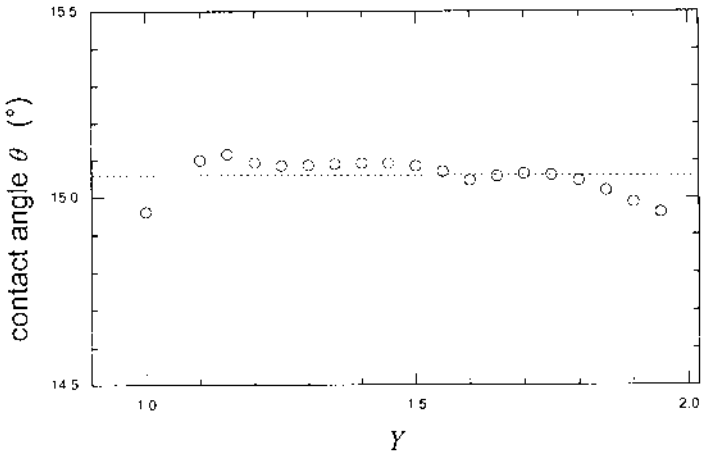

FIG. 12 Results of the L_x,H method applied to the drop profile shown in Fig. 11.

TABLE 1 Results of Contact Angle Determination for the Simulated Drop Profiles Using the Generalized Length–Height Method[a]

	Maximum drop height H[b]			
θ^2	2	3	5	7
5	5.10 ± 0.82	5.03 ± 0.65	4.95 ± 0.75	5.06 ± 0.88
10	10.05 ± 0.50	9.99 ± 0.37	9.98 ± 0.39	10.02 ± 0.51
20	19.95 ± 0.40	20.00 ± 0.20	20.02 ± 0.23	20.02 ± 0.28
30	29.96 ± 0.16	29.99 ± 0.18	30.01 ± 0.12	30.03 ± 0.30
40	40.03 ± 0.27	40.01 ± 0.18	40.01 ± 0.15	40.01 ± 0.18
50	49.94 ± 0.61	50.04 ± 0.14	50.01 ± 0.12	50.01 ± 0.16

[a] The y-coordinates of the theoretical dimensionless drop profiles were overlapped with random errors ranging from −0.025 to 0.025. The results are shown here as average value ± standard derivation, which were evaluated from 40 simulations (cf. text).
[b] The listed H- and θ-values are the values used to generate the theoretical dimensionless drop profiles.
Source: From Ref. 20.

Carbon fibers were tightened to a metal frame using dental cement. Droplets of polymer melts (as shown in Fig. 13) can be prepared by first dipping a tightened fiber into the polymer powder, followed by slowly heating the "powdered" fiber in a hot stage to melt the polymer. Droplets form on the fiber from a receding movement and, therefore, the measured contact angles are (or approaching) their receding angles. The drop images were recorded using a microscope equipped with a digital camera. The images shown here were taken from above (i.e., top view) and it was ensured that all fibers were

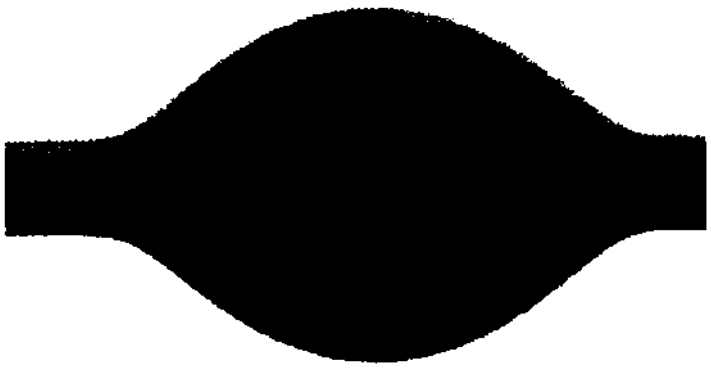

FIG. 13 Image of a polyimide melt droplet resting on a carbon fiber at 420°C.

lying horizontally, perpendicular to the microscope lenses. The drop profiles were extracted from the images using a subpixel routine, as for instance described in Ref. 35. The extracted profiles (Fig. 14) were then used for calculating the contact angles.

The results of the L_y,H method applied to the real carbon fiber/Pl drop profile are shown in Fig. 15. Both sides of the drop profile as well as their averaged profile were used to calculate the contact angles.

Other than the theoretical simulations described above the contact angle values calculated using L_x,H-values in case of the experimentally obtained drop profile are quite sensitive to the X-levels by X approaching 1 (Fig. 15). Nevertheless, as X increases to values around 1.5–3.0 the calculated contact angle values are less dependent on X. The sensitivity of the calculated θ-values against X by small X-values reveals the difficulty in determining the L_x-values near the liquid–fiber contact surface. This might be partially due to the weakness of the program employed. However, the fact that the three-phase contact points in a drop-on-fiber system are often smeared out to some extent is certainly a dominant factor which usually makes an accurate determination of the L_x-value near the contact line rather difficult. This sensitive range is generally more significant for drops having small contact angles as compared to those with large contact angles. The results suggest that contact values determined using the common maximum drop length-height L,H method might deviate significantly from their real values. The L_x,H-values in the X-

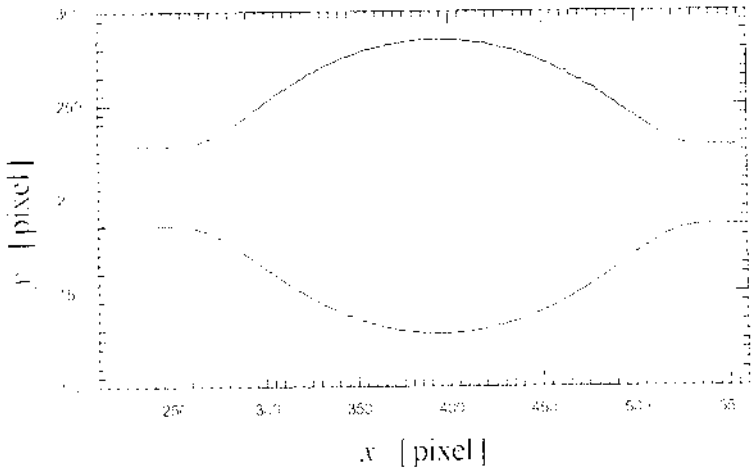

FIG. 14 Extracted profile of the polyimide melt droplet (Fig. 13) resting on a carbon fiber at 420°C.

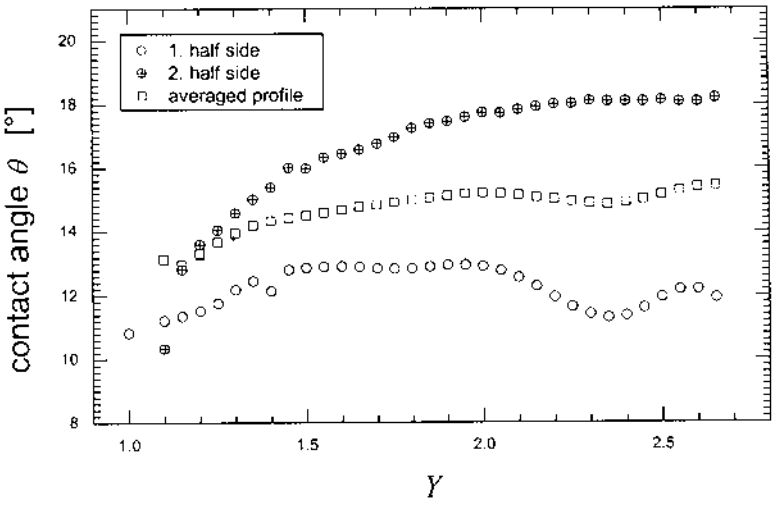

FIG. 15 Results of the L_x,H method applied to the Pl melt droplet profile shown in Fig. 14.

range of 1.5 to 3.0 usually produce more reliable contact angle values. Using average-side profiles rather than simply the single-side profiles of a droplet improves the reliability of calculation even further. The difference between the contact angles obtained from the two-side profiles of a droplet is not due to the possible influence of the gravity on the drop profiles, because the drop images are recorded from above (i.e., top view). It is more likely due to the geometrical asymmetry (see Fig. 16) and/or the chemical heterogeneity of the fibers.

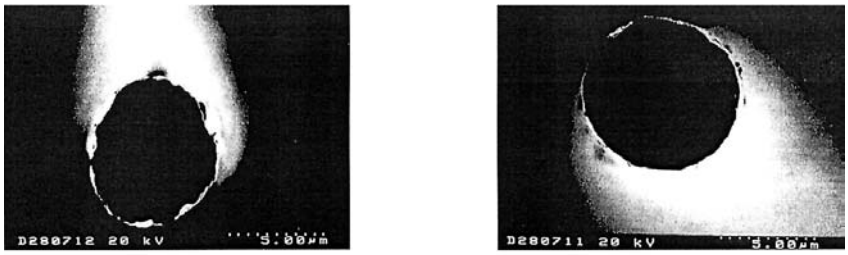

(a) original carbon

(b) in HNO_3 for 24h oxidized carbon fiber

FIG. 16 SEM micrographs of carbon fiber cross sections (fiber diameter).

For experimental applications, care should be taken that optical aberrations and distortions of the drop images are considered (i.e., corrected) in the calculation as far as possible. Image distortions have a rather strong influence on the resulting values because the calculated contact angles are very sensitive to the drop dimensions (see also Fig. 3). Usually, the total image distortions will be summarized into an aspect ratio factor, which has to be determined for each experimental set-up using, for instance, the procedure described in Ref. 35. Further care should be taken to ensure that the fibers are positioned at right angles to the microscope lenses to avoid extra image distortions.

IV. INDIRECT CONTACT ANGLE MEASUREMENTS

Direct methods for the determination of the contact angles from profiles of droplets resting on fibers are also quite difficult to perform, which is related to the tricky handling of thin fibers and small liquid volumes. They are also restricted to fibers with almost perfect circular cross sections. Furthermore, the accuracy of some of the aforementioned methods is directly related to the accuracy of determining the exact position of the three-phase contact point (compare Fig. 17) and the fiber diameter.

The contact angle range that is usually accessible for direct measurements of the contact angle in symmetric drop-on-fiber systems is $0° < \theta < 60°$ [28]. However, if it is possible to control the droplet size, it should be possible to create droplets of a suitable size for optimum direct measurements of the contact angle from drop profiles. For higher contact angles and smaller liquid

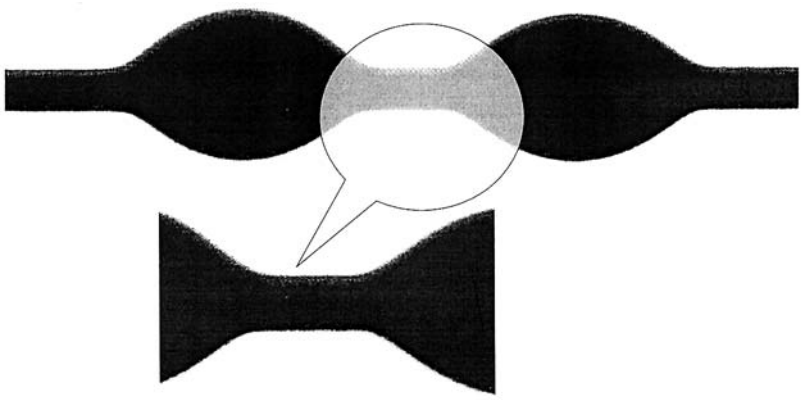

FIG. 17 Image of a polyimide melt droplets resting on a carbon fiber at 420°C. Who would be able to determine exactly the three-phase contact point?

volumes the clam-shell (or asymmetric) configuration of the droplets on fibers becomes more favorable [6,29], which makes it even more difficult to determine the contact angles accurately. In cases where the asymmetric droplet conformation is preferred, it is essential to ensure that the fiber has been rotated to present the exact meridional profile of the droplet to the observer. In cases where this cannot be guaranteed, the determined apparent contact angles will deviate significantly from the real contact angles [1].

In the following section the focus is on the methods that allow the characterization of the wetting behavior indirectly: the contact angle is derived by measuring the wetting force exerted from a meniscus of a liquid on a vertical fiber or by determining the penetration rates of liquids in fiber assemblies.

A. The Modified Wilhelmy Method

The modified Wilhelmy technique [7,30,31] for measuring contact angles θ between fibers and liquids with known surface tensions γ_{lv} or for determining the fiber or filament perimeter and the increase of the fiber perimeter by swelling [7] in a test liquid was introduced several decades ago. This method is very sensitive for measuring contact angles between fibers and low-viscose liquids and is most widely used in all areas where fiber wetting is of interest. The method has been reviewed several times [32,33].

A schematic setup of the Wilhelmy balance is shown in Fig. 18. The fiber is attached to the arm (or using a sample carrier) of a high-precision ultra-

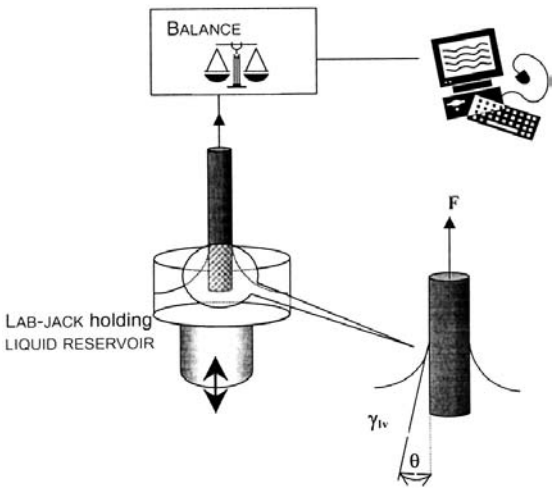

FIG. 18 Schematic of a Wilhelmy balance for measuring contact angles on fibers.

microbalance placed on an antivibration table in an enclosed measuring chamber (in order to avoid undesirable interference in the measured signal due to percussion, drafts, and adsorption of environmental contaminants). The fiber(s) can be immersed into/withdrawn from the test liquid using a reversible elevator platform carrying the beaker containing the liquid, and the mass change detected at the balance will be recorded using a computer. The Wilhelmy method is very accurate, because a balance can be exactly calibrated using calibration weights.

Using the Wilhelmy technique the wetting tension ($\gamma_{lv}\cdot\cos\theta$) exerted by a liquid meniscus on a vertical fiber can be measured directly, using the balance:

$$\gamma_{lv} \cdot \cos\theta = \frac{\Delta m \cdot g}{\pi \cdot d_f} \tag{34}$$

where $\Delta m \cdot g$ is the measured "apparent wetting force" (Δm is the change in "mass" before and after the fiber is immersed in the liquid), g is the acceleration due to gravity and d_f is the fiber diameter. In the case of small fibers with diameters $d_f \leq 50$ μm the buoyant weight of the immersed fiber is negligible and only the capillary term accounts. However, the accuracy of the measurement depends strongly on the accuracy of the determined fiber diameter (or more exactly the determined fiber perimeter). The diameter can be measured easily with the Wilhelmy method using a test liquid which is known to wet the fiber completely (usually *n*-alkanes*), i.e., $\cos\theta = 1$, but only if penetration of the liquid into the fiber can be excluded. In the most practical cases the total absence of contact-angle hysteresis is a convenient test for complete wetting. In this case Eq. (34) becomes:

$$d_f = \frac{\Delta m \cdot g}{\pi \cdot \gamma_{lv}}. \tag{35}$$

The accuracy of the diameter determination depends only on the accuracy of the liquid surface tension γ_{lv}, which can be measured with high precision using the pendent drop method [34,35].

Alternatively, fiber diameters can be measured using scanning electron microscopy (SEM) [36] or optical microscopy equipped with a calibrated

*When using alkanes it is important to ensure that all surface-active impurities are removed from the hydrocarbon. Alkanes can be easily purified by passing them several times through adsorbent columns (i.e., in the case of hydrocarbons the most efficient adsorbent will be basic alumina). The purity of the hydrocarbon can be checked by measuring the hydrocarbon–water interfacial tension [Aveyard R.; Haydon, D.A. Trans. Faraday Soc. 1965, *61*, 2255], which is very sensitive to those impurities [Goebel A.; Lunkenheimer, K. Langmuir 1997, *13*, 369].

eyepiece [37] (but these techniques are only applicable for fibers that do not swell in the test liquid [38]) by averaging the measured diameters for several fibers.

If the receding contact angle is zero (for instance, for water receding contact angles on wood fibers [39]), the following equation has been used to determine advancing contact angles θ_a:

$$\cos \theta_a = \frac{F_a}{F_r} \tag{36}$$

where F_a and F_r are the advancing and receding dynamic wetting forces, respectively. The above equation suggests that the advancing contact angle can be measured without knowing the fiber perimeter [38,40].

When measuring contact angles on very small single fibers, the detectable mass change Δm due to capillary rise on a "monofilament" will be very small. The accuracy of the measurement can be improved by using more than one monofilament. Thus disturbing effects through surface roughness and -heterogeneities and varying fiber perimeters will be averaged out [36,38]. However, care has to be taken that all fibers are placed perpendicular with respect to the liquid surface and parallel to each other on to an appropriate sample holder. The holder should be preferably made of a low-energy material, such as Teflon, in order to avoid problems related to vapor adsorption.

The modified Wilhelmy technique can be used to measure either static or dynamic contact angles. In the static mode the fiber is immersed into the test liquid only by a few millimeters in order to avoid possible end-effects. Afterwards, the fiber is held stationary until a constant mass is measured so that the contact angle can be calculated. In the dynamic mode, however, the mass change is recorded during the whole fiber immersion–emersion cycle at a constant stage velocity. Advancing θ_a and receding θ_r contact angles can be calculated using the Wilhelmy equation from the mass changes, which were detected during the immersion and emersion, respectively, of the fibers into and from the test liquid [Eq. (34)]:

$$\cos \theta = \frac{\Delta m \cdot g}{\pi d_f \cdot \gamma_{lv}} \tag{37}$$

A typical example of the measured weight changes during dynamic contact angle measurements between carbon fibers and water as well as diiodomethane (DIM) is shown in Fig. 19. No buoyancy slope can be observed, even when using more fibers because of the small fiber diameter (around 7 μm) [41].

The ability to measure dynamic contact angles has a major advantage. It enables us to characterize a large surface area of fibers and, therefore, to

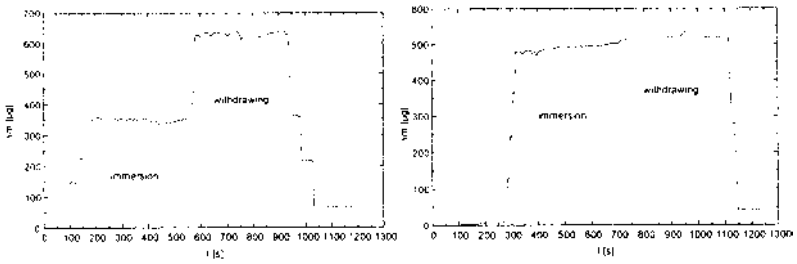

FIG. 19 Typical weight recordings as a function of time during fiber immersion and emersion procedure for four carbon fibers in water (left) and DIM (right).

detect local changes in the wetting behavior. When measuring dynamic advancing and receding contact angles it is possible to study the (chemical) surface heterogeneity [42] and roughness* or kinetic effects such as liquid penetration into the fibers by means of the ubiquitous contact angle hysteresis (for further details see Refs. [43–46]) and, therefore, study fiber swelling, adsorption–desorption processes [47], or in the case of polymer fibers, polymer surface dynamics (due to overturning of molecular segments at the surface). Because of all omnipresent inhomogeneities of fiber surfaces, the measurements have to be repeated several times in order to check the reproducibility of obtained contact angles.

As the solid surface tension γ_s cannot be measured directly, contact angles are, in many cases, used to estimate (calculate) the solid surface tension. Different approaches, all based on the Young equation but on different models for obtaining solid–liquid-interfacial tension γ_{sl} from their surface tension properties (γ_{sv} and γ_{lv} as well as their components), are available to calculate solid surface tensions from measured contact angles [48,49]. The debate still continues over the usage of different approaches in estimating solid surface tensions from experimental contact angle values [50–54]. The majority of these approaches require more than one contact angle to be measured between a studied solid and several test liquids of known surface tension components (or parameters). Test liquids with known surface tension components and parameters can be found in the literature [4,55–59].

*Differently sized glass fibers were characterized using atomic force microscopy and contact angle measurements, it was concluded that roughness plays only a minor roll in causing hysteresis whereas the chemical heterogeneity plays the major part [Wolff, V.; Perwuelz, A.; El Achari, A.; Caze C.; Carlier, E. J. Mater. Sci. 1999, *34*, 3821].

If one is only interested in the solid surface tension and its dispersive (London forces) and polar components, these values can be easily obtained, using the tensiometric method (based on the modified Wilhelmy method) and a two-liquid system (i.e., different hydrocarbons and formamide) [60]. However, in order to obtain "true" surface tension values, one has to ensure that no thin wetting film of the low dense (hydrocarbon) phase will remain after passing through it, before immersing into the higher dense phase (formamide) and vice versa. Such a remaining wetting film acts as a barrier, which prevents a true liquid–fiber contact [60].

1. Some Examples

The modified Wilhelmy method has been frequently used to determine the wetting behavior of fiber materials, ranging from natural fibers [61] to all kinds of synthetic fibers [62]. The method was used (and still is) for the characterization of the changes in the surface chemistry of carbon [63–67], glass [68,69], and natural [70–72] fibers after modifying the fibers, applying sizings and coatings [73] and grafting processes [74–76] as well as for characterizing all kinds of polymer fibers [77,78] regarding their solid surface tension.

Besides wettability the modified Wilhelmy technique used in the dynamic mode also offers the opportunity to study and quantify the swelling properties of modified (polyacrylic acid grafted) and unmodified regenerated cellulose fibers [79]. Measurements of single-fiber swelling give accurate values of the fiber swelling capacity. Such measurements performed on single fibers exclude information about liquid adsorption between the fibers that occur in fiber assemblies. As mentioned above, the accuracy of the contact angles measured using the Wilhelmy method strongly depends on the accuracy of the fiber perimeters. Therefore it was stated that the Wilhelmy method is hardly applicable in the case of natural fibers considering their wide variation in perimeters and shapes [1,80]. The surface tension of cellulose-type fibers can, however, be determined using a simple floating technique using polar (water–methanol) and nonpolar (1-methylnaphthalene/octane) liquid mixtures avoiding contact angle measurements [80].

V. STUDY OF FIBER SURFACE CHEMISTRY BY CONTACT ANGLE MEASUREMENTS

Hüttinger et al. [81] suggested that the acidity and basicity of (carbon) fiber surfaces could be characterized by determining the work of adhesion/pH diagram (Fig. 20). Advancing contact angles are measured using the modified Wilhelmy technique between fiber and acidic and basic aqueous solutions, with varying pH values ranging from 1 to 14. The method is based on the fact that the surface tension and the Lifshitz (L)/van der Waals (W) component of

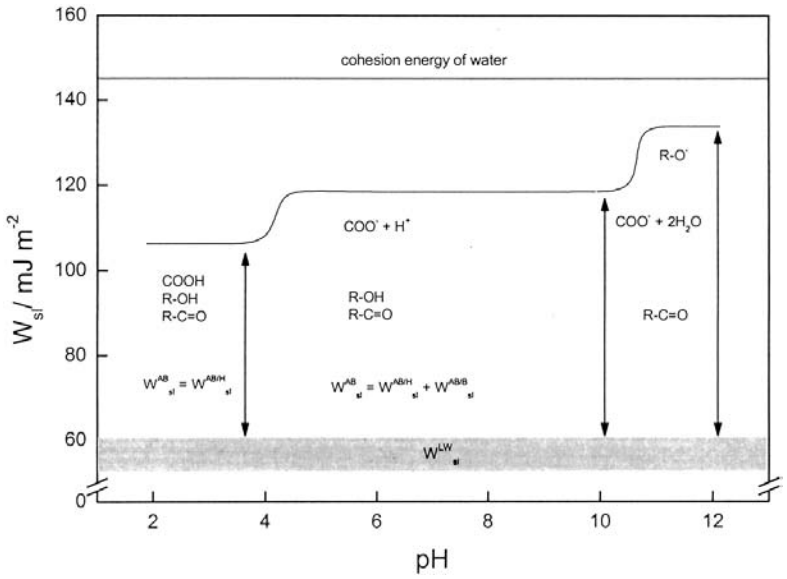

FIG. 20 Schematic work of adhesion/pH diagram including a model for interpreting such a diagram according to Ref. [82].

the surface tension γ_l^{LW} of pure water are not, or only slightly, affected by the addition of small amounts of inorganic acids and bases. This behavior is explained by the strong self-association of the water molecules due to hydrogen bonds. These bonds are practically unaffected by additional ion–dipole interactions. Contact angle measurements as a function of pH can be a valuable tool for analyzing surface functionalities having different pK_a values [82].

The work of adhesion between the solid and aqueous solution W_{sl} depends on the pH value and is composed of a constant contribution due to dispersion (or Lifshitz–van der Waals) interactions W_{sl}^{LW} and different contributions deriving from acid (A)–base (B) interactions W_{AB}^{sl} between the functional groups at the solid–water interface:

$$W_{sl} = W_{sl}^{LW} + W_{sl}^{AB} \tag{38}$$

The acid–base interactions include the formation of Brønsted acid–base complexes ($W_{sl}^{AB/B}$) but also hydrogen bonds ($W_{sl}^{AB/H}$):

$$W_{sl}^{AB} = W_{sl}^{AB/H} + W_{sl}^{AB/B} \tag{39}$$

W_{sl}^{AB} may be calculated, or at least explained, by the following expression:

$$W_{sl}^{AB} = -f \cdot n_i^{AB} \cdot \Delta H_i^{AB} \tag{40}$$

where ΔH_i^{AB} is the enthalpy of the complex or adduct formation of a Brønsted acid–base pair, n_i^{AB} is the number of the acid–base pairs i and f is a correlation factor to correct enthalpy values to free energy values (≈ 1), as the work of adhesion is equivalent to a free energy.

The W_{sl}^{LW} component of the surfaces under investigation can be determined by contact angle measurements, using a nonpolar liquid as the interaction of a nonpolar liquid is restricted to dispersive forces [83]. The nonpolar liquid should have a high surface tension (such as DIM) to avoid the spreading of the liquid. In the case of negligible acid–base interactions (i.e., for nonpolar solids), the total work of adhesion W_{sl} between a solid and a liquid corresponds to W_{sl}^{LW}:

$$W_{sl} = W_{sl}^{LW} = \gamma_l(1 + \cos\theta) \tag{41}$$

Knowing the value of W_{sl}^{LW} and the London–van der Waals component γ_l^{LW} of the liquid surface tension, the same component for the solid surface tension γ_s^{LW} can be calculated using the geometric mean expression:

$$W_{sl}^{LW} = 2\sqrt{\gamma_s^{LW} \cdot \gamma_l^{LW}} \tag{42}$$

If the adsorption of the probe liquid vapor on the solid surface is negligible, $\gamma_s{}^{LW}$ can also be determined, in analogy to the acid–base approach for estimating solid surface tensions [84], by measuring the contact angle of a neutral, non-self-associating liquid (i.e., DIM, squalene, or *n*-alkanes) using the following expression:

$$\gamma_s{}^{LW} = \frac{\gamma_l^{LW}(1 + \cos\theta)^2}{4}. \tag{43}$$

Brønsted acid–base complexes may be formed selectively between surface functional groups and aqueous solutions with different pH values. The free energy of the acid–base complex formation [Eq. (40)] causes an increase in W_{sl} and therefore a step in the W_{sl}/pH diagram. The increased W_{sl} causes the contact angles to decrease. However, it was found that the overall W_{sl} is mainly determined by hydrogen bonds and to a smaller content by well-defined Brønsted acid–base complexes [82]. At very low pH values the hydrogen bonds form between carboxyl-, hydroquinone-, hydroxyl-, phenol-, and carbonyl groups on fiber surfaces and water [82]. With increasing pH values Brønsted acid–base complexes will form. The increase in W_{sl} cannot be large, because the contribution of the hydrogen bonds formed by carboxyl groups

at lower pH values is simultaneously reduced by the formation of carboxylate anions. An analogous interpretation can be given for the second step in the basic range. Brønsted acid–base complexes will be formed between phenolic-OH functional groups and the basic solution medium.

The acidic and basic aqueous solutions to be used in these measurements can simply be prepared by adding hydrochloric acid and sodium hydroxide to water, but other acids and bases might be used alternatively.

Zielke et al. [83] concluded that neither temperature-programmed desorption of functional groups nor quantitative X-ray photoelectron spectroscopy can give absolute information about the exterior surface functionalities on a fiber surface, because both techniques include subsurface contributions. Interactions between the functionalities on the outer fiber surface and test liquids (including aqueous solutions with varying pH values), however, affect the measurable contact angles [85].

VI. CHARACTERIZING FIBER–SURFACTANT INTERACTIONS BY CONTACT ANGLE MEASUREMENTS

Contact angle measurements can also be used to obtain information about adsorption of surfactants on solid surfaces (in our case on fiber materials). In such a case contact angles have to be measured as a function of the surfactant concentration c. Under certain circumstances, but generally if the liquid–vapor surface tension γ_{lv} is larger than the solid surface tension γ_s, no adsorption of the liquid vapor on the solid surface takes place, and therefore the solid surface tension will stay constant with changing surfactant concentration. The Young equation [Eq. (3)] becomes therefore:

$$-\frac{d\gamma_{sl}}{dc} = \frac{d(\gamma_{lv}\cos\theta)}{dc}. \tag{44}$$

It follows the Gibbs equation for solid–liquid interfaces:

$$\Gamma_{sl} = \frac{1}{RT}\frac{d(\gamma_{lv}\cos\theta)}{d\ln c}, \tag{45}$$

where Γ_{sl} is the excess concentration at the solid surface, T is the temperature, and R is the gas constant.

Information about the surfactant adsorption at solid–liquid interfaces can now be obtained by measuring the contact angle as a function of the surfactant concentration [31,86]. However, in many practical applications the direct measurable results are sufficient enough.

The modified Wilhelmy method has been used to follow time-dependent adsorption processes of surfactants from aqueous solutions onto modified and untreated glass fibers [30] and to study interactions between fibers and surfactants [31,38,87,88].

VII. WETTING OF FIBERS BY POLYMER MELTS

The interfacial properties and the flow of polymer melts are important in many technological processes such as polymer blending, fiber, and wire coating as well as in composite manufacturing. In the area of fiber reinforced polymers the nature of the fiber–polymer melt (or prepolymer solution) interface plays a fundamental role, as the adhesive strength of the desired composite material depends strongly on the interphase between both materials. Load stress must be transferred from the matrix through the interphase into the reinforcing fiber. Therefore the wettability of reinforcing fibers by polymer melts or prepolymers (such as resins and vinylesters) is a crucial issue. Poor wetting of the fibers by the liquid matrix will lead to the formation of voids in the fiber–solidified polymer matrix interphase, which will reduce the final strength of the final composite. According to adhesion theories, a thermodynamic prerequisite for good adhesion is that the liquid (the adhesive, i.e., the liquid matrix material) wets the adherend (i.e., the reinforcement). In order for this to happen, the surface tension of the fiber has to be higher than that of the liquid. The fiber surface tension is indirectly accessible by "standard" contact angle measurements vs. test liquids. The wetting kinetic of fibers by the liquid matrix or polymer melts can be characterized by wetting force measurements using the Wilhelmy method [89,90]. However, it is still difficult to obtain directly experimental data about the kinetics of the formation and the interactions in a fiber–high viscose polymer melt interphase [91,92].

Until the present day, only very few methods are available for the study of the wetting behavior of fibers directly by polymer melts. The modified Wilhelmy technique [89,93] can be used to measure directly the wetting tension ($\gamma_{lv} \cdot \cos\theta$). When the surface tension of the polymer melt is known, then the contact angle can be calculated [94]. In addition, direct measurement methods can be used. Such methods enable the calculation of the contact angle of drop-on-fiber systems from the drop shape [18–20].

The first attempts to measure contact angles between a thermoplastic melt (polypropylene) and graphite-, Kevlar-, and glass fibers using the modified Wilhelmy technique were made by Chang and coworkers [95]. Since then, several developments have taken place to improve the Wilhelmy equipment for measuring either the surface tension of polymer melts [89] or the contact angle between single fibers and polymer melts [93,94,96]. The latest descrip-

tion of a new refined device (Fig. 21) to measure the wetting properties of fibers by polymer melts was given by Grundke et al. [93,97]. The experimental setup allows the characterization of polymer melts and the wetting behavior of thin fibers (with diameters in the range 8 μm $< d_f <$ 100 μm) up to 300 °C in an inert gas (Ar) atmosphere [98]. This device is furthermore equipped with two windows that enable parallel imaging of the fiber polymer melt meniscus using a CCD camera.

The major problem when measuring the contact angles between polymer melts and fibers (besides the difficulties of thermal convection currents affecting the balance signal, polymer oxidation, degradation, or crosslinking) is the high melt viscosity. Therefore not only surface tension (capillary) but also hydrodynamic effects have to be considered [89,99]. Two factors determine the rate and extent of the equilibrium of the fiber–melt menisci [89]. First, when using small fibers the meniscus will equilibrate more rapidly (the meniscus height is directly proportional to the fiber diameter on small diameter fibers [89]). The second effect, related to the first, is due to the relative rate of impurities adsorbing at the moving, equilibrating contact line. If small fibers ($d_f <$ 100 μm) are used as the Wilhelmy probe the dimensions of the wetting meniscus between fiber and polymer melt are reduced, which accelerates the equilibration rate [94]. Sauer [94] measured the time needed for a meniscus to equilibrate. The measurements were performed at 23 °C using dry glass fibers having different diameters (8.1 μm $\leq d_f \leq$ 155 μm) and poly(dimethylsiloxane)

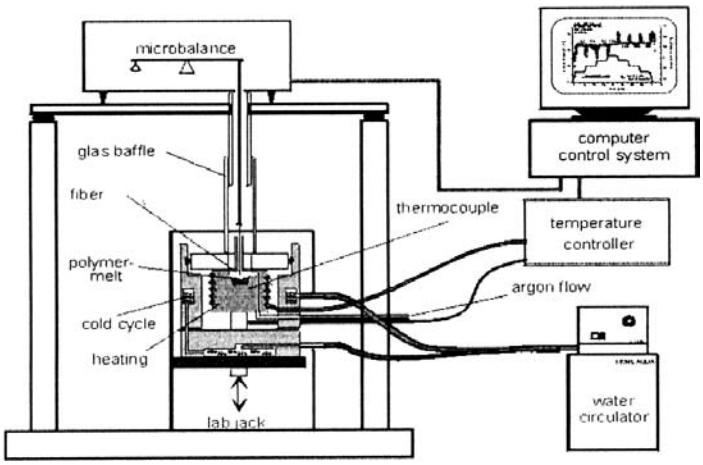

FIG. 21 Schematic of an apparatus allowing the determination of surface tensions of polymer melts by immersing fibers based on the modified Wilhelmy principle [98].

(PDMS) with different viscosities (from 50 mPas to 5 Pas) and found that equilibrium state is established in less than 200 sec between fibers with diameters of $d_f \leq 155$ μm and a high molecular weight PDMS with a viscosity of 5 Pas. In the case of polymeric melts, the time to reach the equilibrium can take up to several minutes for a polypropylene melt on approx. 60 μm glass fibers at temperatures above $T > 160°C$ [93].

VIII. CONTACT ANGLE MEASUREMENTS ON FIBROUS ASSEMBLIES (WOVEN FABRICS, MAT, AND BUNDLES)

Because fibers are in most cases gathered either in rovings (fiber bundle) or as woven textiles, fabrics or mats, and also for these fibrous assemblies, the interaction with liquids, their wetting behavior, is important for manufacturing processes (e.g., dyeing and finishing, sizing, impregnation in composite making) as well as performance or maintenance in use (e.g., washing processes). However, when characterizing the wetting behavior of fabrics, it is not clear whether the wetting should be measured using single fibers taken from the fabric or on fibrous assemblies itself [100]. If the fibers have an irregular surface, in case of natural fibers, both the fiber diameter and the contact angle will vary making it inapplicable to use for instance the Wilhelmy-technique [1]. Furthermore, contact angles measured on single fibers are influenced by the uneven distribution of coatings and sizings after applying fiber treatments. Single-fiber measurements should not be applicable when fiber assemblies have been treated, coated, or sized with a binder [100]. For several processes, such as fiber reinforced polymer composite manufacturing, a number of fibers are wetted simultaneously and therefore measurements on single fibers do not always reflect the "real world."

In the case of woven textiles the interactions with liquids are more complex. They involve several physical phenomena, such as wetting of the fiber surfaces, spontaneous flow of a liquid into an assembly of fibers driven by capillary forces (wicking), adsorption on the fiber surface, and possibly diffusion of the liquid into the interior of the fibers [101]. In general, fiber assembly–liquid interactions depend on the wettability of the fibers, their surface geometry, the capillary geometry of the fabric, the nature of the test liquid, and external forces (applied pressure) [101].

There are different test methods available, which allow the characterization of the wicking behavior of fibrous assemblies, such as the canvas disk wetting test, the Draves test, the demand wetting test, and the Lennox–Kerr test or sinking float test. Kissa [101] reviewed these techniques and the theoretical basics of wetting and wicking of such fiber assemblies. Therefore we

want to concentrate here only on methods that permit the measurement of at least advancing contact angles or the characterization of the fiber assemblies with regard to their surface tension.

A. Contact Angle Measurements and Retention Properties of Woven Fabrics

Hsieh and Yu [102] describe a method to measure simultaneously the liquid wetting and retention characteristics of single-component woven textile fabrics. For the measurements, defined strips (in size and fiber alignment) have to be cut out of the fabric using a die cutter. Each specimen has to be weighted before being attached to a film tab. The tab contains a hole to attach the fabric to the arm of an electronic balance. A commercial tensiometer or a balance (Fig. 18) can be used. The weight of the sample (including the holder) is tarred on the balance. Afterwards, the surface of liquid contained in a reservoir will be raised slowly until it almost touches the sample edge (about 1 mm), then the measurement is started. Upon the first force detection the liquid level is to be stopped. The weight-force recording is to continue until a steady state in the measurement can be established. Then, the fabric will be withdrawn from the test liquid at a higher stage speed until the entire specimen is pulled out of the liquid. After the fabric is completely separated from the liquid a residual weight can be detected, indicating the total liquid retention (W_t), i.e., the amount of liquid retained in the vertical hung fabric. During the measurement, wetting and wicking processes will be detected simultaneously. Therefore the wetting component has to be decoupled from the measurement. The steady state is a combined result of both these processes. Knowing W_t the wetting force F_w can simply be decoupled from the steady state or stabilized balance reading (ΔB_{st}):

$$F_w = (\Delta B_{st} - W_t) \cdot g, \tag{46}$$

where g is the gravitational acceleration and F_w is the vertical attraction force exerted on the fabric as it immerses into the liquid and is expressed as:

$$F_w = \gamma_{lv} \cdot P \cdot \cos\theta \tag{47}$$

where P is the perimeter of the liquid–fabric interface or its wetted length, which can be measured, as described above, using a liquid that will totally wet the fibers (such as alkanes).

$$P = \frac{F_w}{\gamma_{alkanes}} \tag{48}$$

Therefore if the dimensions of the fabric, its wetted length, P, and the liquid surface tension γ_{lv} are known, the advancing contact angle between the fabric and the test liquid θ_a can be calculated.

The alkane retention is used as a measure for the liquid retention capacity of the fabrics (C_m). C_m can also be expressed by the weight ratio of the absorbed liquid over the dry fabric weight [g/g]:

$$C_m = \frac{\rho_l}{\rho_f} \frac{\Phi}{1 - \Phi}, \tag{49}$$

where ρ_l is the liquid density, ρ_f is the fiber density, and Φ is the porosity of the fabric. Φ is defined as the fraction of void space in a porous medium:

$$\Phi = 1 - \frac{\rho_b}{\rho_f}, \tag{50}$$

here ρ_b is the "fabric bulk density," which can be calculated as follows:

$$\rho_b = \frac{\text{fabric weight}}{\text{thickness}} \left[\frac{\text{g/cm}^2}{\text{cm}}\right]. \tag{51}$$

In order to validate their measuring procedure, Hsieh and Yu [102] performed measurements using 100% cotton fabrics of different geometry (warp and werf direction, fabric size, and wetting perimeter) at varying depth of immersion of the fabric into water. The amount of liquid rise in a fibrous assembly depends not only on the wetting property of the fibers but also on the geometric configurations of the pores (capillaries) in the assembly. Their measured data, however, confirmed that the water contact angles are independent of the actual wetted length, i.e., the liquid-substrate perimeters. There was no evidence either that liquid meniscus affects the measured contact angles on fabrics (including woven fabrics, yarns, and fibers). They compared the measured contact angles on a variety of fabrics (natural and synthetic textile fibers) with the wetting properties of single fibers. They found that the contact angles obtained for fabrics and single fibers were identical and that neither the existence nor the magnitude of liquid retention (W_t) interferes with the determination of the contact angle from fabrics [103]. The error range was broader for contact angles in the case of contact angle measured on single fibers extracted from a fabric. Dimensional irregularities along the cotton fiber axis and in cross-sectional shapes complicate the measurements and thus affect the contact angles measured for single fibers. Greater variations in the measured contact angle might also be due to the inhomogeneous character of the fiber surfaces and therefore varying fiber surface wettability.

This method was also applied in the study of the influence of scouring and bleaching on the wetting behavior of slivers, yarns, and plain and satin weave fabrics [104]. In summary, the method introduced by Hsieh and Yu should be applicable for measuring contact angles between liquids and different kinds of fiber assemblies and for estimating the liquid retention behavior as well as the "porosity" of such fabrics.

B. Capillary-Penetration Method or Rising-Height- or Imbibition Technique

The modified Washburn or capillary-rise method can be used to characterize the wetting behavior not only of porous solids [105], powders [106,107] but also of fiber assemblies [108–110], such as rovings or yarns, fabrics, and mats, or at least their surface tension. Different experimental techniques are available for characterizing fiber assemblage. All of them are based on measuring either the weight gain due to liquid penetration as a function of time [111–114] or the penetration time needed for a liquid to rise to a certain height (known as thin-layer wicking technique) [115,116].

C. The Rising-Height or Capillary-Rise Method

Fiber bundles or rovings can be characterized with respect to their wettability or, more or less directly, their surface tension using the rising-height method, which was introduced for porous solids or powders. Apart from the preparation of reproducible fiber "bundles," the same capillary penetration method for powder beds can be used [113]. In this case, a precisely weighted quantity of fibers has to be inserted reproducibly into a sample holder. The packed sample holder will be attached to an electrobalance or a commercial tensiometer and brought into contact with the test liquid. As soon as the sample touches the liquid surface, the immersion movement has to be stopped. Upon the first force detection the liquid level is stopped at almost no immersion of the holder. Then, the penetration velocity of the test liquid into the fiber bundle is determined by recording the weight gain (which is proportional to the capillary height of the liquid front) as a function of time using a computer until a steady state in the measurement is established. Depending on the nature of both the fibers and the test liquid, the measurement can be stopped after a few tens of seconds (typically after 10 to 60 sec). After this time, the deviation of the experimental data from the expected theoretical weight-time dependence increases drastically. This renders any additional data useless with respect to the data evaluation, according to the Washburn equation. The deviations are caused by 1) gravity, which hinders the liquid from

penetrating into the solid with increasing penetration height; and 2) by evaporation of the test liquid (if the liquid is volatile enough) [113]. After completing the measurement, the sample holder can be withdrawn from the test liquid and residual weight indicating the total liquid retention can be determined.

The evaluation of the measured data is based on modifications [111] of the Washburn equation [117] for a single capillary, which arises from the combination of expression for the Laplace pressure and the Hagen–Poiseuille equation for steady flow conditions.

$$\gamma_{lv} \cos \theta = \left[\frac{2}{A^2 r}\right]\left[\frac{\eta}{\rho^2}\right]\left[\frac{m^2}{t}\right] \tag{52}$$

where A is the cross-sectional area and r is the radius of the capillary, η is the liquid viscosity, ρ is the liquid density, m is the weight of the liquid which penetrates into the capillary, and t is the time.

However, in the case of short fiber beds or fiber bundles the geometry of the capillary system is unknown and therefore the factor $[2/A^2 r]$ has to be replaced by an unknown factor $1/C$, which leads to:

$$C \cdot \gamma_{lv} \cos \theta = \left[\frac{\eta}{\rho^2}\right]\left[\frac{m^2}{t}\right]. \tag{53}$$

The factor $[\eta/\rho^2]$ reflects the properties of the test liquid and $[m^2/t]$ is measured using a balance or tensiometer.

This modified Washburn equation can be used under the following assumptions: 1) laminar flow is predominating in the pore spaces; 2) gravity is negligible; and 3) the geometry of the porous solid–fiber bundle is constant [112].

As experimental result we obtain the weight increase m as a function of the square root of time $\sqrt{t}$ (or the weight increase m^2 as a function of time t). By determining the slope of the linear part of these plots (see also the example shown in Fig. 22), we can obtain the needed experimental quantity $[m^2/t]$.

If this quantity is measured for a series of different test liquids, the surface tension of the solid (fiber bundle, powder, or porous solid) can be determined. Because $[m^2/t][\eta/\rho^2]$ equals $C{\cdot}\gamma_{lv} \cos \theta$ according to Eq. (53), $C{\cdot}\gamma_{lv} \cos \theta$ can be plotted vs. the liquid-surface tension γ_{lv} of the test liquids used. This plot (see Fig. 23) will show a maximum that is analogous to Zisman's critical solid–vapor surface tension γ_c of the investigated material [108,113].

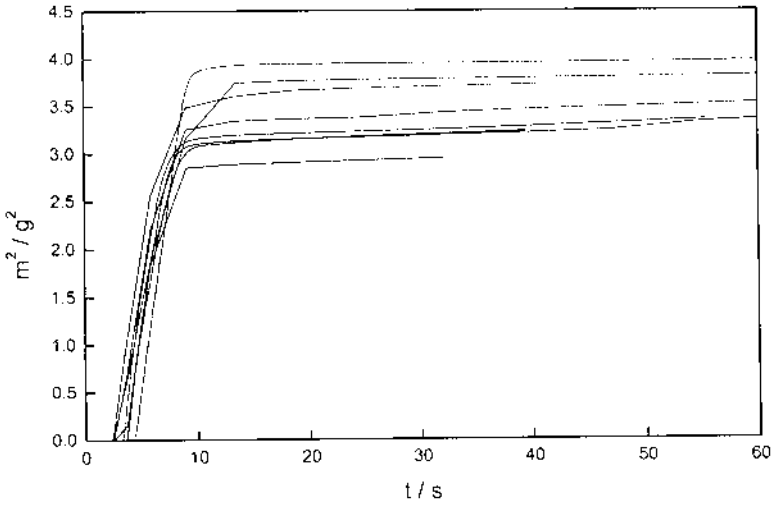

FIG. 22 Weight rise curves of *N*,*N*-dimethyl formamide into cellulose fibers as a function of time. (From Ref. 118.)

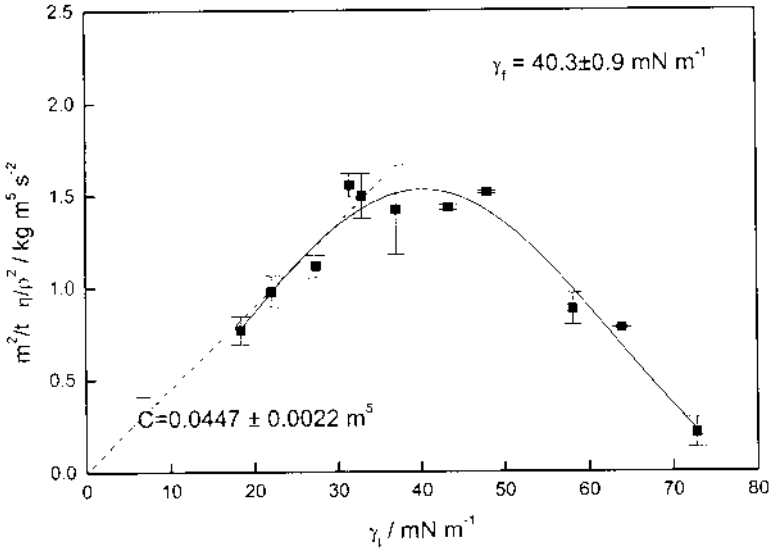

FIG. 23 Plot of the normalized wetting rates as a function of the test liquid surface tension for pure cellulose. (From Ref. 118.)

On the other hand, if one needs to determine contact angles using the capillary-rise method, the constant C can be determined assuming a mean capillary radius r_c and a corresponding number of capillaries n_c

$$C = \frac{\pi^2}{2} \cdot r_c^5 \cdot n_c^2 \tag{54}$$

with an "extra" measurement using a liquid that will completely wet the solid under investigation, as for instance hexane. Assuming complete wetting, therefore $\cos\theta = 1$, C can be determined using the following equation [119]

$$C = \left[\frac{\eta}{\gamma_{lv} \cdot \rho^2}\right]\left[\frac{m^2}{t}\right]. \tag{55}$$

After measuring the weight increase due to the penetration of the test liquid of interest into the solid, the contact angle can be calculated as follows, assuming C is really a constant:

$$\cos\theta = \left[\frac{1}{C\gamma_{lv}}\right]\left[\frac{\eta}{\rho^2}\right]\left[\frac{m^2}{t}\right] \tag{56}$$

Additionally, an averaged constant C can also be determined from the plot of the normalized wetting rate $C{\cdot}\gamma_{lv}\cos\theta$, which is the raw wetting rate $[m^2/t]$ multiplied by the term containing the liquid properties $[\eta/\rho^2]$, over the liquid-surface tension γ_{lv}; as long as the liquids wet the solid completely and, therefore, the contact angle is zero, a straight line graph through the origin having the slope C results. If $\theta > 0$, deviations from the curve to lower values occur [108]. As exemplarily shown for cellulose fibers in Fig. 23, C can be determined by a linear fit through the origin to the data on the left-hand side of the maximum, assuming that all these liquids still wet the solid completely.

The measured normalized wetting rates for various test liquids (for cellulose fibers; Fig. 23) can be transformed into the cosine of the contact angle ($\cos\theta$) and plotted as a function of the liquid surface tension (Fig. 24). The resulting linear relationship $\cos\theta = 1 - b(\gamma_l - \gamma_c)$ was established empirically by Zisman and Fox [120] and found to hold for solid with low surface tensions. The critical surface tension γ_c corresponds to the surface tension of the liquid that will just spread over/wet completely the solid. The constant C reflects the capillary geometry of the "porous solid" and may change in a non-predictable manner during the penetration process of different test liquids. It was concluded from the experiments performed [112] that there is no need to determine the constant C in order to obtain solid-surface tensions, because the position of the maximum in the $C{\cdot}\gamma_{lv}\cos\theta$ vs. γ_{lv} plot, which is expected to

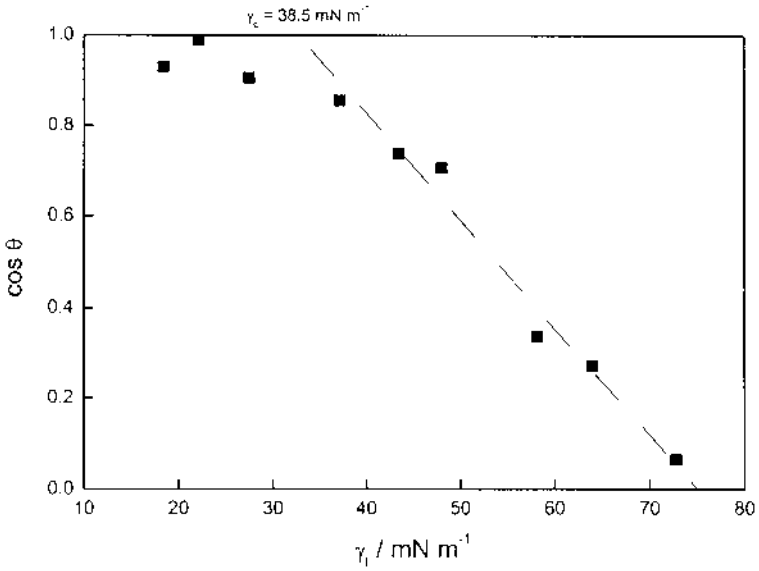

FIG. 24 Zisman plot for estimating the cellulose fiber surface tension (the cosines of the contact angles were extracted from the measured normalized wetting rates) using the averaged constant $\bar{C}$ determined from Fig. 23. (From Ref. 118.)

reflect the solid-surface tension, is not affected by the sample geometry. However, Chibowski and Perea-Carpio [121] state that this "apparently interesting approach should be carefully considered, because for low energy nonpolar (or weakly polar) solid many approaches give reasonable agreement just because the surface energy is low."

D. Some Examples

The capillary-rise technique [108] as described above was successfully applied to characterize differently sized glass fibers [91] and modified jute fibers [70] with respect to their surface tensions. Gassan et al. [70] found that the packing density of the fibers influences only slightly the measured contact angle. However, in the case of hydrophilic natural fibers the measured contact angle is affected by the diffusion of the test liquid into the fibers. The measured $[m^2/t]$ function contains not only information about the wetting process but also about the absorption of the liquid, the penetration of the test liquid into the fibers. Swelling takes place and therefore the fiber diameter increases, which again influences the geometry factor C, which influences the contact angle. Significant differences were found comparing the surface-tension values cal-

culated from the contact angles determined using the capillary-rise technique and the modified Wilhelmy method [70].

Bubert et al. [122] recently reported on successful contact angle measurements between carbon nano-fibers ($50 < d_f < 200$ nm) with length of 40 mm and test liquids using the "powder-method by which a constant volume of nanofibers are given into a capillary." However, they reported only surface tension values and no contact angle data and nothing about the accuracy of the measurements in the paper.

E. The Thin-Layer Wicking Technique

The thin-layer wicking technique has been used to characterize textile fabrics with respect to their surface tension γ_s (based on the acid–base approach [84]). The technique is based on the Washburn equation and was originally introduced by Giese et al. [115] and later modified by Chibowski and Holysz [116]. The method was found to be especially suitable for characterizing (strips of) textile fabrics [123,124] and the process of surfactant and dye adsorption by the fabrics [125–127].

The modified Washburn equation [116,128] relates the changes in the surface free energy ΔG connected to the replacement of the solid–gas by a solid–liquid interface during the wicking process:

$$x^2 = \frac{r_p \cdot t}{2\eta} \cdot \Delta G. \tag{57}$$

In a typical experiment the time t that a liquid with a viscosity η needs to travel a certain distance x through a textile having an "effective pore radius" r_p has to be measured at a constant temperature [116,129].

Chibowski and Holysz [116,130] considered four cases, in which ΔG has different values:

(i) A low surface tension liquid, such as *n*-alkanes, completely wets a surface that is equilibrated with the liquid's saturated vapor for a sufficiently long time (a duplex film has formed), then $\Delta G = \gamma_{lv}$ and the original form of the Washburn equation can be used:

$$x^2 = \frac{r_p \cdot t}{2\eta} \cdot \gamma_{lv} \tag{58}$$

The measured function $x^2 = f(t)$ allows determining the "effective pore radius" r_p parameter.

(ii) $\Delta G = W_{sl} - W_{ll}$ in the case of using the same set of liquids as described in case (i) now spreading/wetting the "bare" surface (not precontacted with the liquid vapor). $W_{sl}\,[=\gamma_{lv}(1+\cos\theta)]$ and $W_{ll}\,(=2\gamma_{lv})$ are

the thermodynamic work of adhesion between the liquid and the solid and the liquid's work of cohesion, respectively.
Using the formulations of the acid–base approach of interfacial interactions [84,131] we find:

$$\Delta G = 2\sqrt{\gamma_s^{LW}\gamma_{lv}^{LW}} + 2\sqrt{\gamma_s^{+}\gamma_{lv}^{-}} + 2\sqrt{\gamma_s^{-}\gamma_{lv}^{+}} - 2\gamma_{lv} \tag{59}$$

where γ^{LW} is the Lifshitz–van der Waals component of the surface tension, γ^{+} is the electron acceptor/proton donor (acidity parameter) and γ^{-} is the electron donor/proton acceptor (basicity parameter) according to van Oss et al. [84]. The subscripts s and l always indicate solid and liquid, respectively.

(iii) A liquid is not completely wetting the solid that was equilibrated with the liquid vapor, and a dynamic contact angle θ, which is not the Young contact angle on a flat solid [132], appears at the liquid penetration front and $\Delta G = \gamma_{lv}\cos\theta$.

(iv) $\Delta G = \gamma_{lv}\cos\theta + W_{sl} - W_{ll}$, if the same liquid as in case (iii) is wetting the "bare" nonpreequilibrated solid surface. Using the acid–base approach to estimate the solid surface tension we obtain:

$$\Delta G = \gamma_{lv}\cos\theta + 2\sqrt{\gamma_s^{LW}\gamma_{lv}^{LW}} + 2\sqrt{\gamma_s^{+}\gamma_{lv}^{-}} + 2\sqrt{\gamma_s^{-}\gamma_{lv}^{+}} \tag{60}$$

Once the "effective pore radius" parameter r_p was determined [Eq. (58)] in a first experiment using a liquid with known surface tension γ_{lv} and viscosity that wets the solid completely, it will be possible, according to Refs. [116,128, 130], to use the appropriate ΔG-values from cases (iii) and (iv) to determine the solid surface tension components.

All nonpolar liquids (*n*-alkanes or DIM) interact with solid surface only via long range, Lifshitz–van der Waals forces γ_{lv}^{LW}, and, therefore, applying the acid–base approach formulations Eq. (59) becomes:

$$\Delta G = W_{sl} - W_{ll} = 2\sqrt{\gamma_s^{LW}\gamma_{lv}^{LW}} - 2\gamma_{lv} \tag{61}$$

Now, using "bare" samples in an *n*-alkane wicking experiment, the driving force for liquid penetration, according to case (ii), should be $\Delta G = W_{sl} - W_{ll}$. The Lifshitz–van der Waals component of the solid surface tension γ_s^{LW} can be calculated by combining Eqs. (57) and (61). Another way to determine γ_s^{LW} is by using high surface tension nonpolar liquids, e.g., DIM. We then measure the functions $x^2 = f(t)$ for the "bare" and preequilibrated solid considering the cases (iii) and (iv). The value of $\Delta G = \gamma_{lv}\cos\theta$ from case (iii) will be determined and introduced into the equation of case (iv), assuming that γ_{lv}

cos θ is equal in the two cases. Solving the equations for cases (iii) and (iv) simultaneously allows the determination of γ_s^{LW}.

The electron acceptor γ^+ and electron donor γ^- parameters of the solid (and, therefore, the acid–base component $\gamma^{AB} = 2\sqrt{\gamma^+\gamma^-}$) can be determined using polar liquids with known surface tension components and parameters (see for instance Refs. [58,59,131,133]), as well as viscosities for the liquid penetration experiments and considering the proper experimental conditions (i) to (iv). Again, the functions $x^2 = f(t)$ for the "bare" and preequilibrated solid have to be measured separately, and ΔG_{bare} as well as ΔG_{pre} has to be determined according to Eq. (58). The following Eq. (62) needs to be solved to estimate the γ^+ and γ^- parameters:

$$\Delta G_{bare} - \Delta G_{pre} = 2\sqrt{\gamma_s^{LW}\gamma_{lv}^{LW}} + 2\sqrt{\gamma_s^+\gamma_{lv}^-} + 2\sqrt{\gamma_s^-\gamma_{lv}^+} - 2\gamma_{lv} \tag{62}$$

The experiments can be performed as follows [116,123,124,130]: The fabric of interest is to be placed on a glass plate. The strip must be slightly strained to guarantee uniform porosity for the penetrating liquids. In order to obtain the solid surface tension components and parameters from such thin-layer wicking experiments, the latter have to be conducted not only on bare (cleaned and dried) fabric strips but also on strips that were preequilibrated with the test liquid's vapor. The equilibration of the fabric strips with the saturated liquid vapors can be performed for instance in desiccators containing the appropriate liquid on the bottom for a certain period of time at the measuring temperature.

The thin-layer wicking experiments have to be performed in a closed sandwich chamber in which the glass plate (containing the fiber strip) is to be placed in an exactly horizontal position. The chamber lid (if not the whole chamber) should be made from glass, so that the moving boundary of the liquid penetration front in the strip is visible. On the edges of the sandwich chamber there has to be a scale, which allows the recording of the penetration time. The test liquid is transported from the bottles to the "porous layer" using a flannel wick. The liquid surface has to be on the same level as the testing plate in the sandwich chamber. One end of the flannel wick is dipped into the liquid and the other will be attached to the end of the plate when starting the penetration experiment.

All the above-described forms of the Washburn equation [cases (i) to (iv)] should result in a straight-line dependence for $x^2 = f(t)$, having different slopes depending on the true free energy changes accompanying the liquid penetration into the fabric (or any porous solid medium) [116]. Deviations from the linearity of the $x^2 = f(t)$ relationship could occur if the (apparent) contact angle changes during the penetration process or if a nonuniform liquid front develops due to a nonuniform distribution of the pore size of the

fabric [134]. However, it was recently shown by a mathematical analysis of the Washburn equation that most of discordance found from its application is due to the inadequate use of this equation [135]. It was proposed to use the Washburn equation as a polynomial expression instead of its linearized form. In the proposed way the deviation from linearity will disappear [135].

Note again: The contact angle appearing under these dynamic conditions is not expected to be the equilibrium Young contact angle [132]. Therefore it is not possible to calculate a "Young" contact angle using the modified Washburn equation [case (iii)]:

$$\cos\theta = \frac{x^2}{t}\,\frac{2\eta}{r_p \cdot \gamma_{lv}} \tag{63}$$

for a liquid with known surface tension and viscosity, but not completely wetting the solid, penetrating a porous medium with known "effective pore radius" [116,136].

IX. OTHER METHODS TO MEASURE CONTACT ANGLES ON FIBERS

In addition to the aforementioned techniques, most commonly used for the characterization of fibers, fiber assemblies, and fabrics in terms of their wetting behavior or surface tension, there are also other methods available: the determination of the contact angle from the equilibrium meniscus near a floating fiber [80], the reflection method initially developed by Jones and Porter [137] (reviewed in Refs. 1 and 32), the tilted fiber or rotating stage technique [138,139], and the solidification front method (recently reviewed in Ref. 140).

A comparison between contact angles of various test liquids (glycerol and water) on carbon- and Kevlar fibers measured using the solidification front technique and the modified Wilhelmy method can be found in Ref. 141. The results obtained using both techniques are consistent with each other, which illustrates that both techniques will produce reliable data for small-diameter fibers. However, the solidification technique offers a number of potential advantages compared to the modified Wilhelmy method [140]. This is because it is not possible to measure the fiber diameter and the contact angle simultaneously with the Wilhelmy method. Also, in cases where the fibers have a nonuniform character it becomes even more difficult. The fiber geometry may also influence the results, so that a convoluted fiber cross section can cause wicking effects and therefore lead to incorrect balance readings [140].

APPENDIX: Contact Angle (θ) as a Function of the Maximum Drop Height (H) and Length (L)

H	0°	5°	10°	15°	20°	25°	30°	35°	40°
1.50	7.7750	6.8605	5.9460	5.1230	4.4240	3.8465	3.3725	2.9825	2.6590
1.55	7.9170	7.0655	6.2020	5.4065	4.7145	4.1305	3.6435	3.2370	2.8955
1.60	8.0590	7.2610	6.4405	5.6710	4.9880	4.4010	3.9030	3.4825	3.1265
1.65	8.1990	7.4460	6.6645	5.9195	5.2465	4.6585	4.1530	3.7210	3.3510
1.70	8.3380	7.6240	6.8770	6.1545	5.4925	4.9050	4.3940	3.9520	3.5700
1.75	8.4765	7.7965	7.0795	6.3780	5.7270	5.1415	4.6260	4.1760	3.7840
1.80	8.6140	7.9650	7.2740	6.5920	5.9515	5.3695	4.8510	4.3940	3.9930
1.85	8.7510	8.1280	7.4615	6.7975	6.1675	5.5885	5.0685	4.6060	4.1965
1.90	8.8880	8.2880	7.6425	6.9955	6.3755	5.8010	5.2795	4.8125	4.3960
1.95	9.0225	8.4435	7.8190	7.1870	6.5770	6.0065	5.4850	5.0135	4.5915
2.00	9.1575	8.5970	7.9905	7.3730	6.7720	6.2065	5.6845	5.2105	4.7830
2.05	9.2915	8.7485	8.1580	7.5540	6.9620	6.4005	5.8795	5.4030	4.9705
2.10	9.4250	8.8980	8.3220	7.7305	7.1470	6.5900	6.0700	5.5910	5.1545
2.15	9.5575	9.0445	8.4830	7.9025	7.3275	6.7750	6.2560	5.7755	5.3350
2.20	9.6900	9.1900	8.6410	8.0715	7.5040	6.9560	6.4385	5.9565	5.5130
2.25	9.8215	9.3335	8.7965	8.2370	7.6770	7.1335	6.6170	6.1340	5.6875
2.30	9.9525	9.4755	8.9500	8.3995	7.8465	7.3070	6.7925	6.3090	5.8595
2.35	10.084	9.6170	9.1010	8.5595	8.0130	7.4775	6.9645	6.4805	6.0290
2.40	10.214	9.7560	9.2500	8.7170	8.1765	7.6455	7.1340	6.6495	6.1960
2.45	10.343	9.8950	9.3975	8.8720	8.3380	7.8105	7.3010	6.8160	6.3605
2.50	10.472	10.033	9.5430	9.0250	8.4965	7.9730	7.4650	6.9805	6.5230
2.55	10.601	10.169	9.6875	9.1760	8.6530	8.1330	7.6270	7.1425	6.6835
2.60	10.729	10.305	9.8300	9.3255	8.8075	8.2910	7.7870	7.3020	6.8420
2.65	10.857	10.439	9.9715	9.4730	8.9605	8.4470	7.9445	7.4600	6.9990
2.70	10.984	10.573	10.112	9.6195	9.1110	8.6010	8.1005	7.6160	7.1540
2.75	11.111	10.706	10.251	9.7640	9.2605	8.7535	8.2545	7.7705	7.3070
2.80	11.238	10.838	10.389	9.9075	9.4080	8.9040	8.4065	7.9230	7.4590
2.85	11.364	10.970	10.527	10.050	9.5540	9.0535	8.5575	8.0740	7.6095
2.90	11.490	11.101	10.663	10.191	9.6990	9.2010	8.7065	8.2240	7.7580
2.95	11.615	11.231	10.798	10.330	9.8425	9.3470	8.8545	8.3720	7.9055
3.00	11.740	11.361	10.932	10.468	9.9850	9.4920	9.0010	8.5190	8.0520
3.05	11.865	11.490	11.066	10.606	10.126	9.6355	9.1460	8.6645	8.1970
3.10	11.989	11.619	11.199	10.743	10.266	9.7785	9.2900	8.8090	8.3410
3.15	12.113	11.747	11.331	10.880	10.405	9.9195	9.4330	8.9525	8.4840
3.20	12.237	11.875	11.463	11.015	10.543	10.060	9.5745	9.0945	8.6255
3.25	12.361	12.002	11.594	11.149	10.681	10.200	9.7150	9.2355	8.7665
3.30	12.484	12.128	11.724	11.283	10.817	10.338	9.8550	9.3755	8.9060
3.35	12.607	12.255	11.853	11.415	10.952	10.476	9.9935	9.5150	9.0450
3.40	12.729	12.381	11.983	11.547	11.087	10.612	10.132	9.6530	9.1830
3.45	12.852	12.506	12.111	11.678	11.221	10.748	10.269	9.7905	9.3200
3.50	12.974	12.631	12.239	11.809	11.354	10.883	10.405	9.9270	9.4565
3.55	13.096	12.756	12.367	11.940	11.487	11.017	10.540	10.063	9.5920
3.60	13.217	12.880	12.494	12.069	11.619	11.151	10.675	10.198	9.7270
3.65	13.339	13.004	12.620	12.198	11.750	11.284	10.809	10.333	9.8610

45°	50°	55°	60°	65°	70°	75°	80°	85°	90°
2.3875	2.1565	1.9585	1.7865	1.6360	1.5025	1.3830	1.2760	1.1785	1.0900
2.6070	2.3605	2.1475	1.9620	1.7985	1.6540	1.5240	1.4075	1.3015	1.2045
2.8225	2.5610	2.3340	2.1355	1.9605	1.8045	1.6650	1.5390	1.4240	1.3195
3.0330	2.7580	2.5185	2.3075	2.1210	1.9545	1.8050	1.6700	1.5470	1.4345
3.2395	2.9520	2.7000	2.4780	2.2805	2.1040	1.9450	1.8010	1.6700	1.5500
3.4420	3.1430	2.8795	2.6465	2.4390	2.2525	2.0845	1.9320	1.7930	1.6655
3.6405	3.3310	3.0570	2.8135	2.5960	2.4005	2.2235	2.0630	1.9160	1.7810
3.8355	3.5155	3.2320	2.9785	2.7515	2.5470	2.3620	2.1930	2.0390	1.8970
4.0265	3.6975	3.4045	3.1420	2.9060	2.6930	2.4995	2.3230	2.1615	2.0125
4.2140	3.8770	3.5750	3.3040	3.0595	2.8380	2.6365	2.4530	2.2840	2.1285
4.3985	4.0535	3.7435	3.4640	3.2115	2.9820	2.7730	2.5820	2.4060	2.2440
4.5800	4.2275	3.9100	3.6225	3.3625	3.1255	2.9090	2.7105	2.5280	2.3595
4.7580	4.3995	4.0745	3.7795	3.5120	3.2675	3.0440	2.8390	2.6500	2.4750
4.9335	4.5685	4.2370	3.9350	3.6605	3.4090	3.1785	2.9670	2.7715	2.5905
5.1065	4.7355	4.3975	4.0890	3.8075	3.5495	3.3125	3.0945	2.8930	2.7060
5.2770	4.9005	4.5565	4.2420	3.9535	3.6890	3.4460	3.2215	3.0135	2.8210
5.4450	5.0635	4.7140	4.3930	4.0985	3.8280	3.5785	3.3480	3.1345	2.9360
5.6105	5.2245	4.8695	4.5430	4.2425	3.9660	3.7105	3.4740	3.2545	3.0510
5.7740	5.3840	5.0235	4.6915	4.3855	4.1030	3.8415	3.5995	3.3750	3.1655
5.9355	5.5410	5.1765	4.8390	4.5275	4.2390	3.9725	3.7245	3.4945	3.2800
6.0950	5.6970	5.3275	4.9855	4.6685	4.3745	4.1025	3.8495	3.6140	3.3945
6.2530	5.8510	5.4775	5.1305	4.8085	4.5095	4.2320	3.9735	3.7330	3.5085
6.4090	6.0035	5.6260	5.2740	4.9475	4.6435	4.3610	4.0975	3.8520	3.6225
6.5635	6.1550	5.7730	5.4170	5.0855	4.7770	4.4890	4.2210	3.9705	3.7360
6.7160	6.3045	5.9190	5.5590	5.2230	4.9095	4.6170	4.3440	4.0885	3.8495
6.8675	6.4530	6.0640	5.7000	5.3595	5.0415	4.7445	4.4665	4.2065	3.9630
7.0175	6.6000	6.2080	5.8395	5.4950	5.1725	4.8710	4.5885	4.3240	4.0760
7.1660	6.7460	6.3505	5.9785	5.6300	5.3035	4.9970	4.7105	4.4415	4.1890
7.3130	6.8910	6.4920	6.1165	5.7640	5.4335	5.1230	4.8320	4.5585	4.3020
7.4590	7.0345	6.6325	6.2540	5.8975	5.5625	5.2480	4.9530	4.6755	4.4145
7.6040	7.1770	6.7725	6.3905	6.0300	5.6915	5.3730	5.0735	4.7920	4.5270
7.7475	7.3185	6.9115	6.5260	6.1625	5.8195	5.4970	5.1935	4.9080	4.6390
7.8905	7.4590	7.0490	6.6605	6.2935	5.9475	5.6210	5.3135	5.0240	4.7510
8.0320	7.5990	7.1860	6.7950	6.4245	6.0745	5.7445	5.4330	5.1395	4.8630
8.1725	7.7375	7.3225	6.9280	6.5545	6.2010	5.8675	5.5525	5.2550	4.9745
8.3120	7.8755	7.4580	7.0610	6.6840	6.3275	5.9900	5.6715	5.3705	5.0860
8.4510	8.0125	7.5925	7.1930	6.8130	6.4530	6.1120	5.7900	5.4850	5.1970
8.5885	8.1485	7.7265	7.3240	6.9415	6.5780	6.2340	5.9080	5.6000	5.3085
8.7255	8.2840	7.8600	7.4550	7.0690	6.7025	6.3550	6.0260	5.7145	5.4190
8.8620	8.4185	7.9925	7.5850	7.1965	6.8270	6.4760	6.1435	5.8285	5.5300
8.9970	8.5525	8.1245	7.7145	7.3230	6.9505	6.5970	6.2610	5.9425	5.6405
9.1320	8.6855	8.2555	7.8435	7.4495	7.0740	6.7170	6.3780	6.0565	5.7510
9.2660	8.8180	8.3865	7.9715	7.5750	7.1970	6.8370	6.4950	6.1700	5.8615
9.3990	8.9500	8.5165	8.0995	7.7005	7.3195	6.9565	6.6115	6.2830	5.9715

(*Continued on next page*)

APPENDIX (Continued)

H	0°	5°	10°	15°	20°	25°	30°	35°	40°
3.70	13.460	13.127	12.746	12.327	11.881	11.416	10.942	10.466	9.9945
3.75	13.580	13.251	12.872	12.455	12.011	11.547	11.075	10.599	10.127
3.80	13.701	13.374	12.998	12.583	12.140	11.678	11.206	10.731	10.259
3.85	13.821	13.496	13.123	12.710	12.269	11.809	11.338	10.863	10.391
3.90	13.942	13.619	13.247	12.837	12.397	11.938	11.468	10.994	10.522
3.95	14.062	13.741	13.371	12.963	12.525	12.068	11.598	11.125	10.652
4.00	14.181	13.863	13.495	13.088	12.653	12.196	11.728	11.254	10.782
4.05	14.301	13.984	13.619	13.214	12.780	12.325	11.857	11.384	10.911
4.10	14.420	14.105	13.742	13.339	12.906	12.452	11.986	11.513	11.040
4.15	14.539	14.226	13.865	13.463	13.032	12.580	12.114	11.641	11.168
4.20	14.658	14.347	13.987	13.587	13.158	12.706	12.241	11.769	11.295
4.25	14.777	14.467	14.109	13.711	13.283	12.833	12.368	11.896	11.423
4.30	14.895	14.588	14.231	13.834	13.408	12.959	12.495	12.023	11.549
4.35	15.014	14.708	14.353	13.958	13.533	13.084	12.621	12.150	11.676
4.40	15.132	14.827	14.474	14.080	13.657	13.209	12.747	12.276	11.802
4.45	15.250	14.947	14.595	14.204	13.781	13.334	12.872	12.401	11.927
4.50	15.368	15.066	14.716	14.325	13.904	13.459	12.997	12.526	12.052
4.55	15.486	15.185	14.837	14.448	14.027	13.583	13.122	12.651	12.177
4.60	15.603	15.304	14.957	14.569	14.150	13.706	13.246	12.776	12.301
4.65	15.720	15.423	15.077	14.690	14.272	13.830	13.370	12.900	12.425
4.70	15.838	15.542	15.197	14.811	14.395	13.953	13.493	13.024	12.549
4.75	15.955	15.660	15.317	14.933	14.516	14.075	13.617	13.147	12.672
4.80	16.072	15.778	15.436	15.053	14.638	14.198	13.739	13.270	12.795
4.85	16.188	15.896	15.555	15.173	14.759	14.320	13.862	13.393	12.917
4.90	16.305	16.014	15.674	15.293	14.880	14.441	13.984	13.515	13.040
4.95	16.421	16.131	15.792	15.414	15.001	14.563	14.106	13.637	13.162
5.00	16.537	16.248	15.911	15.532	15.121	14.684	14.227	13.758	13.283
5.05	16.653	16.366	16.029	15.651	15.241	14.805	14.349	13.880	13.404
5.10	16.769	16.483	16.148	15.771	15.361	14.925	14.470	14.001	13.525
5.15	16.885	16.599	16.266	15.890	15.481	15.046	14.591	14.122	13.646
5.20	17.001	16.716	16.383	16.008	15.601	15.166	14.711	14.243	13.766
5.25	17.117	16.833	16.501	16.128	15.720	15.286	14.831	14.363	13.887
5.30	17.232	16.950	16.618	16.246	15.839	15.405	14.951	14.483	14.007
5.35	17.348	17.066	16.736	16.364	15.958	15.525	15.071	14.603	14.126
5.40	17.463	17.182	16.853	16.482	16.077	15.644	15.191	14.723	14.246
5.45	17.578	17.298	16.970	16.599	16.195	15.763	15.310	14.842	14.365
5.50	17.693	17.414	17.086	16.717	16.313	15.882	15.429	14.962	14.484
5.55	17.808	17.530	17.203	16.834	16.432	16.001	15.548	15.080	14.603
5.60	17.923	17.645	17.320	16.952	16.549	16.119	15.667	15.199	14.722
5.65	18.037	17.761	17.436	17.069	16.667	16.237	15.785	15.318	14.840
5.70	18.152	17.876	17.552	17.185	16.785	16.355	15.904	15.436	14.958
5.75	18.266	17.991	17.668	17.302	16.902	16.473	16.022	15.554	15.076
5.80	18.381	18.107	17.784	17.419	17.019	16.590	16.139	15.672	15.194
5.85	18.495	18.222	17.900	17.535	17.136	16.708	16.257	15.790	15.311
5.90	18.609	18.336	18.015	17.651	17.253	16.825	16.375	15.907	15.429

45°	50°	55°	60°	65°	70°	75°	80°	85°	90°
9.5315	9.0815	8.6460	8.2270	7.8255	7.4415	7.0760	6.7275	6.3965	6.0815
9.6635	9.2120	8.7750	8.3540	7.9500	7.5635	7.1950	6.8435	6.5090	6.1910
9.7950	9.3420	8.9035	8.4800	8.0740	7.6850	7.3135	6.9590	6.6220	6.3010
9.9255	9.4715	9.0310	8.6060	8.1975	7.8060	7.4315	7.0745	6.7345	6.4105
10.056	9.6005	9.1585	8.7315	8.3205	7.9265	7.5495	7.1900	6.8465	6.5200
10.186	9.7290	9.2855	8.8565	8.4435	8.0470	7.6675	7.3050	6.9590	6.6290
10.315	9.8570	9.4120	8.9810	8.5660	8.1670	7.7850	7.4195	7.0710	6.7380
10.443	9.9845	9.5380	9.1055	8.6880	8.2865	7.9020	7.5340	7.1825	6.8470
10.571	10.112	9.6635	9.2290	8.8095	8.4060	8.0190	7.6485	7.2940	6.9560
10.699	10.238	9.7885	9.3525	8.9310	8.5250	8.1355	7.7625	7.4055	7.0645
10.826	10.364	9.9135	9.4755	9.0520	8.6440	8.2520	7.8765	7.5170	7.1730
10.953	10.490	10.038	9.5980	9.1725	8.7625	8.3680	7.9900	7.6280	7.2815
11.079	10.615	10.162	9.7200	9.2930	8.8805	8.4840	8.1035	7.7390	7.3900
11.205	10.740	10.285	9.8420	9.4130	8.9985	8.6000	8.2165	7.8495	7.4980
11.330	10.864	10.408	9.9635	9.5325	9.1165	8.7150	8.3300	7.9600	7.6065
11.455	10.989	10.531	10.085	9.6520	9.2335	8.8305	8.4425	8.0705	7.7145
11.579	11.112	10.654	10.206	9.7715	9.3510	8.9455	8.5555	8.1810	7.8220
11.704	11.235	10.776	10.327	9.8900	9.4675	9.0600	8.6680	8.2910	7.9300
11.827	11.358	10.897	10.447	10.009	9.5845	9.1745	8.7800	8.4010	8.0375
11.951	11.481	11.019	10.567	10.127	9.7010	9.2890	8.8925	8.5110	8.1450
12.074	11.603	11.140	10.687	10.245	9.8170	9.4030	9.0045	8.6210	8.2525
12.197	11.725	11.261	10.806	10.363	9.9330	9.5170	9.1165	8.7305	8.3600
12.319	11.847	11.381	10.925	10.481	10.049	9.6310	9.2280	8.8400	8.4670
12.441	11.968	11.501	11.044	10.598	10.164	9.7445	9.3395	8.9495	8.5745
12.563	12.089	11.621	11.163	10.715	10.280	9.8580	9.4510	9.0585	8.6815
12.684	12.210	11.741	11.281	10.832	10.395	9.9710	9.5620	9.1675	8.7880
12.805	12.330	11.860	11.399	10.948	10.509	10.084	9.6730	9.2765	8.8950
12.926	12.450	11.979	11.517	11.064	10.624	10.197	9.7840	9.3855	9.0020
13.047	12.570	12.098	11.634	11.180	10.738	10.310	9.8950	9.4945	9.1085
13.167	12.689	12.217	11.752	11.296	10.853	10.422	10.005	9.6030	9.2150
13.287	12.809	12.335	11.869	11.412	10.967	10.535	10.116	9.7115	9.3215
13.407	12.928	12.453	11.986	11.528	11.081	10.647	10.226	9.8200	9.4280
13.526	13.047	12.571	12.102	11.643	11.195	10.759	10.336	9.9280	9.5345
13.646	13.165	12.689	12.219	11.758	11.308	10.871	10.446	10.036	9.6405
13.765	13.284	12.806	12.335	11.873	11.422	10.983	10.557	10.144	9.7470
13.884	13.402	12.924	12.451	11.988	11.535	11.094	10.666	10.252	9.8530
14.002	13.520	13.041	12.567	12.103	11.648	11.206	10.776	10.360	9.9590
14.121	13.638	13.157	12.683	12.217	11.761	11.317	10.886	10.468	10.065
14.239	13.755	13.274	12.799	12.331	11.874	11.428	10.995	10.576	10.170
14.357	13.872	13.390	12.914	12.445	11.987	11.539	11.105	10.683	10.276
14.474	13.989	13.507	13.029	12.559	12.099	11.650	11.214	10.791	10.382
14.592	14.106	13.623	13.144	12.673	12.211	11.761	11.323	10.898	10.488
14.709	14.223	13.739	13.259	12.787	12.324	11.872	11.432	11.006	10.593
14.826	14.340	13.854	13.374	12.900	12.436	11.982	11.541	11.113	10.699
14.943	14.456	13.970	13.488	13.013	12.548	12.093	11.650	11.220	10.804

(*Continued on next page*)

APPENDIX (Continued)

H	0°	5°	10°	15°	20°	25°	30°	35°	40°
5.95	18.723	18.451	18.131	17.768	17.370	16.942	16.492	16.025	15.546
6.00	18.837	18.566	18.246	17.884	17.486	17.059	16.609	16.142	15.663
6.05	18.951	18.680	18.361	17.999	17.602	17.176	16.726	16.259	15.779
6.10	19.064	18.795	18.476	18.115	17.719	17.292	16.843	16.375	15.896
6.15	19.178	18.909	18.591	18.230	17.835	17.409	16.959	16.492	16.012
6.20	19.291	19.023	18.706	18.346	17.950	17.525	17.076	16.608	16.129
6.25	19.405	19.137	18.821	18.462	18.066	17.641	17.192	16.725	16.245
6.30	19.518	19.251	18.935	18.576	18.182	17.757	17.308	16.841	16.361
6.35	19.631	19.365	19.050	18.691	18.297	17.873	17.424	16.957	16.476
6.40	19.745	19.479	19.164	18.806	18.412	17.988	17.540	17.073	16.592
6.45	19.858	19.592	19.278	18.920	18.528	18.104	17.655	17.188	16.708
6.50	19.971	19.706	19.392	19.035	18.643	18.219	17.771	17.304	16.823
6.55	20.083	19.819	19.506	19.150	18.758	18.334	17.886	17.419	16.938
6.60	20.196	19.933	19.620	19.264	18.872	18.449	18.001	17.534	17.053
6.65	20.309	20.046	19.734	19.379	18.987	18.564	18.116	17.649	17.168
6.70	20.422	20.159	19.848	19.493	19.102	18.679	18.231	17.764	17.282
6.75	20.534	20.272	19.961	19.606	19.216	18.794	18.346	17.879	17.397
6.80	20.646	20.385	20.075	19.721	19.330	18.908	18.461	17.993	17.511
6.85	20.759	20.498	20.188	19.835	19.444	19.023	18.575	18.108	17.626
6.90	20.871	20.611	20.301	19.949	19.558	19.137	18.690	18.222	17.740
6.95	20.983	20.723	20.415	20.062	19.672	19.251	18.804	18.337	17.854
7.00	21.096	20.836	20.528	20.176	19.786	19.365	18.918	18.451	17.968
7.05	21.208	20.949	20.641	20.289	19.900	19.479	19.032	18.565	18.082
7.10	21.320	21.061	20.754	20.402	20.014	19.593	19.146	18.679	18.195
7.15	21.431	21.173	20.866	20.515	20.127	19.707	19.260	18.792	18.309
7.20	21.543	21.286	20.979	20.629	20.240	19.820	19.374	18.906	18.422
7.25	21.655	21.398	21.092	20.741	20.354	19.934	19.487	19.019	18.536
7.30	21.767	21.510	21.204	20.855	20.467	20.047	19.601	19.133	18.649
7.35	21.878	21.622	21.317	20.967	20.580	20.160	19.714	19.246	18.762
7.40	21.990	21.734	21.429	21.079	20.693	20.274	19.827	19.359	18.875
7.45	22.101	21.846	21.541	21.193	20.806	20.387	19.940	19.472	18.988
7.50	22.213	21.958	21.654	21.305	20.919	20.500	20.053	19.585	19.101
7.55	22.324	22.070	21.766	21.418	21.032	20.613	20.166	19.698	19.213
7.60	22.435	22.181	21.878	21.530	21.144	20.725	20.279	19.811	19.326
7.65	22.547	22.293	21.990	21.642	21.257	20.838	20.392	19.924	19.438
7.70	22.658	22.404	22.102	21.755	21.369	20.951	20.505	20.036	19.551
7.75	22.769	22.516	22.213	21.867	21.481	21.063	20.617	20.149	19.663
7.80	22.880	22.627	22.325	21.978	21.594	21.176	20.730	20.261	19.775
7.85	22.991	22.739	22.437	22.091	21.706	21.288	20.842	20.373	19.887
7.90	23.102	22.850	22.548	22.203	21.818	21.400	20.954	20.486	19.999
7.95	23.213	22.961	22.660	22.314	21.930	21.512	21.066	20.598	20.111
8.00	23.323	23.072	22.771	22.426	22.042	21.624	21.178	20.710	20.223
8.05	23.434	23.183	22.883	22.538	22.154	21.736	21.290	20.822	20.334
8.10	23.545	23.294	22.994	22.649	22.266	21.848	21.402	20.933	20.446
8.15	23.655	23.405	23.105	22.761	22.377	21.960	21.514	21.045	20.558

45°	50°	55°	60°	65°	70°	75°	80°	85°	90°
15.060	14.572	14.085	13.602	13.126	12.660	12.203	11.759	11.327	10.910
15.177	14.688	14.200	13.717	13.239	12.771	12.313	11.868	11.434	11.015
15.293	14.804	14.315	13.830	13.352	12.883	12.424	11.976	11.541	11.120
15.409	14.919	14.430	13.944	13.465	12.994	12.534	12.085	11.648	11.225
15.525	15.035	14.545	14.058	13.578	13.106	12.643	12.193	11.755	11.331
15.641	15.150	14.659	14.172	13.690	13.217	12.753	12.301	11.862	11.436
15.757	15.265	14.774	14.285	13.802	13.328	12.863	12.410	11.968	11.541
15.872	15.380	14.888	14.398	13.915	13.439	12.973	12.518	12.075	11.646
15.988	15.495	15.002	14.511	14.027	13.550	13.082	12.626	12.182	11.751
16.103	15.610	15.116	14.624	14.139	13.660	13.191	12.734	12.288	11.855
16.218	15.724	15.230	14.737	14.250	13.771	13.301	12.841	12.394	11.960
16.333	15.839	15.343	14.850	14.362	13.881	13.410	12.949	12.501	12.065
16.448	15.953	15.457	14.963	14.474	13.992	13.519	13.057	12.607	12.170
16.562	16.067	15.570	15.075	14.585	14.102	13.628	13.165	12.713	12.274
16.677	16.181	15.683	15.187	14.696	14.212	13.737	13.272	12.819	12.379
16.791	16.295	15.796	15.300	14.808	14.322	13.846	13.380	12.925	12.483
16.905	16.408	15.909	15.412	14.919	14.432	13.954	13.487	13.031	12.588
17.019	16.522	16.022	15.524	15.030	14.542	14.063	13.594	13.137	12.692
17.133	16.635	16.135	15.636	15.141	14.652	14.172	13.702	13.243	12.797
17.247	16.748	16.247	15.747	15.251	14.762	14.280	13.809	13.349	12.901
17.361	16.862	16.360	15.859	15.362	14.871	14.389	13.916	13.454	13.005
17.474	16.975	16.472	15.971	15.473	14.981	14.497	14.023	13.560	13.110
17.588	17.088	16.585	16.082	15.583	15.090	14.605	14.130	13.666	13.214
17.701	17.200	16.697	16.193	15.694	15.199	14.713	14.237	13.771	13.318
17.814	17.313	16.809	16.305	15.804	15.309	14.821	14.344	13.877	13.422
17.927	17.426	16.921	16.416	15.914	15.418	14.929	14.450	13.982	13.526
18.040	17.538	17.032	16.527	16.024	15.527	15.037	14.557	14.088	13.630
18.153	17.650	17.144	16.638	16.134	15.636	15.145	14.664	14.193	13.734
18.266	17.763	17.256	16.749	16.244	15.745	15.253	14.770	14.298	13.838
18.379	17.875	17.367	16.859	16.354	15.854	15.361	14.877	14.404	13.942
18.491	17.987	17.479	16.970	16.464	15.962	15.468	14.983	14.509	14.046
18.604	18.099	17.590	17.080	16.573	16.071	15.576	15.090	14.614	14.150
18.716	18.211	17.701	17.191	16.683	16.180	15.683	15.196	14.719	14.254
18.828	18.322	17.812	17.301	16.792	16.288	15.791	15.302	14.824	14.358
18.940	18.434	17.923	17.412	16.902	16.397	15.898	15.408	14.929	14.461
19.052	18.546	18.034	17.522	17.011	16.505	16.005	15.515	15.034	14.565
19.164	18.657	18.145	17.632	17.120	16.613	16.113	15.621	15.139	14.669
19.276	18.768	18.256	17.742	17.230	16.721	16.220	15.727	15.244	14.772
19.388	18.880	18.366	17.852	17.339	16.830	16.327	15.833	15.349	14.876
19.499	18.991	18.477	17.962	17.448	16.938	16.434	15.939	15.453	14.979
19.611	19.102	18.588	18.071	17.557	17.046	16.541	16.045	15.558	15.083
19.722	19.213	18.698	18.181	17.666	17.154	16.648	16.151	15.663	15.186
19.834	19.324	18.808	18.291	17.774	17.262	16.755	16.256	15.768	15.290
19.945	19.435	18.919	18.400	17.883	17.369	16.862	16.362	15.872	15.393
20.056	19.545	19.029	18.510	17.992	17.477	16.968	16.468	15.977	15.497

(*Continued on next page*)

APPENDIX (Continued)

H	0°	5°	10°	15°	20°	25°	30°	35°	40°
8.20	23.766	23.516	23.216	22.872	22.489	22.072	21.626	21.157	20.669
8.25	23.876	23.627	23.328	22.983	22.600	22.183	21.738	21.268	20.780
8.30	23.987	23.738	23.439	23.095	22.712	22.295	21.849	21.380	20.892
8.35	24.097	23.848	23.550	23.206	22.823	22.406	21.961	21.491	21.003
8.40	24.207	23.959	23.660	23.317	22.935	22.518	22.072	21.603	21.114
8.45	24.318	24.069	23.771	23.428	23.046	22.629	22.183	21.714	21.225
8.50	24.428	24.180	23.882	23.539	23.157	22.740	22.295	21.825	21.336

REFERENCES

1. Carroll, B.J. Colloids Surf. A 1993, *74*, 131.
2. Coulson, S.R.; Woodward, I.S.; Badyal, J.P.S.; Brewer, S.A.; Willis, C. Chem. Mater. 2000, *12*, 2031.
3. Rebouillat, S.; Letellier, B.; Steffenino, B. Intern. J. Adhesion Adhes. 1999, *19*, 303.
4. Wu, S. Polymer Interface and Adhesion. Marcel Dekker: New York, 1980.
5. Clint, J.H. Curr. Opin. Colloid Interface Sci. 2001, *6*, 28.
6. McHale, G.; Newton, M.I. Colloids Surf. A 2002, *206*, 79.
7. Collins, G.E. J. Text. Inst. 1947, *38*, T73.
8. Morra, M.; Occiello, E.; Garbassi, F. Adv. Colloid Interface Sci. 1990, *32*, 79.
9. Paynter, R.W. Surf. Interface Anal. 1998, *26*, 674.
10. Berg, J.C. Preface. In *Wettability*; Berg, J.C., Ed.; Marcel Dekker: New York, 1993.
11. Aveyard, R.; Haydon, D.A. *An Introduction to the Principles of Surface Chemistry*; University Press: Cambridge, 1973.
12. Johnson, R.E. Jr.; Dettre, R.H. Surfactant Science. In *Wettability*; Series; Berg, J.C Ed.; Marcel Dekker: New York, 1993; Vol. 49, 1.
13. Fowkes, F.M. Attractive Forces at Solid–Liquid Interfaces. In *Wetting*; S.C.I. Monograph No. 25: London, 1967.
14. Carlson, B.C. SIAM J. Math. Anal. 1977, *8*,231.
15. Carlson, B.C. Numer. Math. 1979, *33*, 1.
16. Wagner, H.D. J. Appl. Phys. 1990, *67*, 1352.
17. Press, W.H.; Teukolsky, S.A.; Vetterling, W.T.; Flannery, B.P. *Numerical Recipes in C (The Art of Scientific Computing)*, 2nd Ed.; Cambridge University Press: Cambridge, 1992.
18. Yamaki, J.; Katayama, Y. J. Appl. Polym. Sci. 1975, *19*, 2897.
19. Carroll, B.J. J. Colloid Interface Sci. 1976, *57*, 488.
20. Song, B.; Bismarck, A.; Tahhan, R.; Springer, J. J. Colloid Interface Sci. 1998, *197*, 68.
21. Gilbert, A.H.; Goldstein, B.; Marom, G. Composites 1990, *21*, 408.

45°	50°	55°	60°	65°	70°	75°	80°	85°	90°
20.167	19.656	19.139	18.619	18.100	17.585	17.075	16.573	16.081	15.600
20.278	19.767	19.249	18.728	18.209	17.693	17.182	16.679	16.186	15.703
20.389	19.877	19.359	18.838	18.317	17.800	17.289	16.785	16.290	15.807
20.500	19.987	19.469	18.947	18.426	17.908	17.395	16.890	16.395	15.910
20.611	20.098	19.578	19.056	18.534	18.015	17.502	16.996	16.499	16.013
20.722	20.208	19.688	19.165	18.642	18.123	17.608	17.101	16.603	16.116
20.832	20.318	19.798	19.274	18.751	18.230	17.714	17.206	16.708	16.220

22. Brochard, F. J. Chem. Phys. 1986, *84*, 4664.
23. De Gennes, P.G. Rev. Mod. Phys. 1985, *57*, 827.
24. Bismarck, A.; Kumru, M.E.; Song, B.; Springer, J.; Moos, E.; Karger-Kocsis, J. Composites A 1999, *30*, 1351.
25. Bismarck, A.; Pfaffernoschke, M.; Song, B.; Springer, J. J. Appl. Polym. Sci. 1999, *71*, 1893.
26. Bismarck, A.; Richter, D.; Wuertz, C.; Springer, J. Colloids Surf. A 1999, *159*, 341.
27. Bismarck, A.; Richter, D.; Wuertz, C.; Kumru, M.E.; Song, B.; Springer, J. J. Adhesion 2000, *73*, 19.
28. Carroll, B.J. J. Adhesion Sci. Technol. 1992, *6*, 938.
29. Carroll, B.J. Langmuir 1986, *2*, 248.
30. Neumann, A.W.; Tanner, W. Proceedings of the Vth Int. Congress on Surface Active Substances; Barcelona, 1968; Vol. II, 727–733.
31. Neumann, A.W. Chem. Ing. Techn. 1970, *42*, 969.
32. Neumann, A.W.; Good, R.J. In *Surface and Colloid Science*; Good, R.J. Stromberg, R.R., Eds.; Plenum Press, New York, 1979; Vol. 11, 31 pp.
33. Bascom, W.D. In *Modern Approaches to Wettability: Theory and Applications*; Schrader, M.E. Loeb, G., Eds.; Plenum Press: New York, 1992; 359 pp.
34. Song, B.; Springer, J. J. Colloid Interface Sci. 1996, *184*, 64.
35. Song, B.; Springer, J. J. Colloid Interface Sci. 1996, *184*, 77.
36. Bismarck, A.; Kumru, M.E.; Springer, J. J. Colloid Interface Sci. 1999, *210*, 60.
37. González-Benito, J.; Baselga, J.; Aznar, A.J. J. Mater. Proc. Technol. 1999, *92–93*, 129.
38. Deng, Y.L.; Abazeri, M. Wood Fiber Sci. 1998, *30*, 155.
39. Hodgson, K.T.; Berg, J.C. Wood Fiber Sci. 1988, *20*, 3.
40. Shen, W.; Sheng, Y.J.; Parker, I.H. J. Adhesion Sci. Technol. 1999, *13*, 887.
41. Bismarck, A. Chemische Modifizierung von Carbonfasern: Elektrokinetische und oberflächenenergetische Charakterisierung/Einfluß auf die Adhäsion zu thermoplastischen Polymeren. dissertation.de: Berlin, 1999.
42. Tagawa, M.; Ohmae, N.; Umeno, M.; Gotoh, K.; Yasukawa, A.; Tagawa, M. Colloid Polym. Sci. 1989, *267*, 702.
43. Johson, R.E. Jr.; Dettre, R.H. In *Contact Angle, Wettability, and Adhesion*.

Advances in Chemistry Series; American Chemical Society: Washington, D.C., 1964, *43*, 112.
44. Dettre, R.H.; Johnson, R.E. Jr. In Contact Angle, Wettability, and Adhesion, Advances in Chemistry Series; American Chemical Society: Washington, D.C., 1964, *43*, 136.
45. Garbassi, F.; Morra, M.; Occhiello, E. *Polymer Surfaces; From Physics to Technology*; John Wiley and Sons: Chichester, 1994; 171 pp.
46. Extrand, C.W.; Kumagai, Y. J. Colloid Interface Sci. 1997, *191*, 378.
47. Uyama, Y.; Inoue, H.; Ito, K.; Kishida, A.; Ikada, Y. J. Colloid Interface Sci. 1991, *141*, 275.
48. Morra, M.; Occhiello, E.; Garbassi, F. Adv. Colloid Interface Sci. 1990, *32*, 79.
49. Kloubek, J. Adv. Colloid Interface Sci. 1992, *38*, 99.
50. Fowkes, F.M.; Riddle, F.L.; Pastore, W.E.; Weber, A.A. Colloids Surf. 1990, *43*, 367.
51. In: *Applied Surface Thermodynamics*; Neumann, A.W., Spelt, J.K., Eds.; Marcel Dekker: New York, 1996.
52. Lyklema, J. Colloids Surf. A 1999, *156*, 413.
53. Della Volpe, C.; Siboni, S. In *Encyclopedia of Surface and Colloid Science*; Hubbard, A., Ed.; Marcel Dekker: New York, 2002; 17 pp.
54. Morra, M. In *Encyclopedia of Surface and Colloid Science*; Hubbard, A., Ed.; Marcel Dekker: New York, 2002; 74 pp.
55. Hammer, G.E.; Drzal, L.T. Appl. Surf. Sci. 1980, *4*, 340.
56. Comyn, J. Adhesion Science; RSC Paperbacks: Cambridge, 1997.
57. Good, R.J.; van Oss, C.J. In *Modern Approaches to Wettability*; Schrader, M.E. Loeb, G.I., Eds.; Plenum Press: New York, 1992; 1 pp.
58. Lee, L.-H. Langmuir 1996, *12*, 1681.
59. Della Volpe, C.; Siboni, S. J. Colloid Interface Sci. 1997, *195*, 121.
60. Schultz, J.; Cazeneuve, C.; Shanahan, M.E.R.; Donnet, J.B. J. Adhesion 1981, *12*, 221.
61. Felix, J.M.; Gatenholm, P. Polym. Composites 1993, *14*, 449.
62. Lu, W.; Fu, X.; Chung, D.D.L. Cem. Concr. Res. 1998, *28*, 783.
63. Tsutsumi, K.; Ishida, S.; Shibata, K. Colloid Polym. Sci. 1990, *268*, 31.
64. Gotoh, K.; Yasukawa, A.; Ohikita, M.; Obata, H.; Tagawa, M. Colloid Polym. Sci. 1995, *273*, 1144.
65. Lee, J.-S.; Kang, T.-J. Carbon 1997, *35*, 209.
66. Bismarck, A.; Springer, J. Colloids Surf. A 1999, *159*, 331.
67. Bismarck, A.; Wuertz, C.; Springer, J. Carbon 1999, *37*, 1019.
68. Wu, H.F.; Dwight, D.W.; Huff, N.T. Composites Sci. Technol. 1997, *57*, 975.
69. Bismarck, A.; Egia-Ajuriagojeaskoa, E.; Springer, J.; Habel, W.R. J. Chim. Phys. 1999, *96*, 1269.
70. Gassan, J.; Bledzki, A.K.; Gutowski, V.S. Materialprüfung 1998, *40*, 93.
71. van de Velde, K.; Kiekens, P. In *Proceedings 2nd International Wood and Natural Fiber Composites Symposium*, Kassel, Germany, 1999; 7-1–7-12 pp.
72. de Meijer, M.; Haemers, S.; Cobben, W.; Militz, H. Langmuir 2000, *16*, 9352.

73. Dilsiz, N.; Wightman, J.P. Carbon 1999, *37*, 1105.
74. Iroh, J.O.; Yuan, W. Polymer 1994, *37*, 4197.
75. Bismarck, A.; Pfaffernoschke, M.; Springer, J. J. Appl. Polym. Sci. 1999, *71*, 1175.
76. Saïhi, D.; El-Achari, A.; Ghenaim, A.; Cazé, C. Polym. Test 2002, *21*, 615.
77. Tagawa, M.; Gotoh, K.; Yasukawa, A.; Ikuta, M. Colloid Polym. Sci. 1990, *268*, 589.
78. Tate, M.L.; Kamath, Y.K.; Wesson, S.P.; Ruetsch, S.B. J. Colloid Interface Sci. 1996, *177*, 579.
79. Karlsson, J.O.; Andersson, M.; Berntsson, P.; Chihani, T.; Gatenholm, P. Polymer 1998, *39*, 3589.
80. van Hazendonk, J.M.; van der Putten, J.C.; Keurentjes, J.T.F.; Prins, A. Colloids Surf. A 1993, *81*, 251.
81. Hüttinger, K.J.; Höhmann-Wien, S.; Krekel, G. Carbon 1991, *29*, 1281.
82. Zielke, U.; Hüttinger, K.J.; Hoffman, W.P. Carbon 1996, *34*, 1007.
83. Zielke, U.; Hüttinger, K.J.; Hoffman, W.P. Carbon 1996, *34*, 999.
84. van Oss, C.J. Interfacial Forces in Aqueous Media. Marcel Dekker: New York, 1994.
85. Zielke, U.; Hüttinger, K.J.; Hoffman, W.P. Carbon 1996, *34*, 1015.
86. Yaminsky, V.V.; Yaminskaya, K.B. Langmuir 1995, *11*, 936.
87. Rhee, H.; Young, R.A.; Sarmadi, A.M. J. Text. Inst. 1993, *84*, 394.
88. Okamura, Y.; Gotoh, K.; Kosaka, M.; Tagawa, M. J. Adhesion Sci. Technol. 1998, *12*, 639.
89. Sauer, B.B.; Diapaolo, N.V. J. Colloid Interface Sci. 1991, *144*, 527.
90. Sauer, B.B.; Kampert, W.G. J. Colloid Interface Sci. 1998, *199*, 28.
91. Mäder, E.; Jacobasch, H.-J.; Grundke, K.; Gietzelt, T. Composites A 1996, *27*, 907.
92. Morra, M.; Occiello, E.; Garbassi, F. Polymer 1993, *34*, 736.
93. Grundke, K.; Uhlmann, P.; Gietzelt, T.; Redlich, B.; Jacobasch, H.-J. Colloids Surf. A 1996, *116*, 93.
94. Sauer, B.B. J. Adhesion Sci. Technol. 1992, *6*, 955.
95. Chang, H.W.; Smith, R.P.; Li, S.K.; Neumann, A.W. Polymer Sci. Technol. Ser. In *Molecular Characterization of Composite Interfaces*; Ishida, H. Kumar, G., Eds.; Plenum Press: New York, 1985; Vol. 27, 413.
96. Kern, T. LaborPraxis 1998, *22*, 48.
97. Jacobasch, H.-J.; Grundke, K.; Augsburg, A.; Gietzelt, T.; Schneider, S. Progr. Colloid Polym. Sci. 1997, *105*, 44.
98. Jenschke, W.; Michel S.; Arnold, D. "Anlage zur Bestimmung der Oberflächenspannung von Polymerschmelzen mittels eintauchender Faser nach dem modifizierten Wilhelmy-Prinzip" link in: http://www.ipfdd.de/frameset.html?./research/equip/equipment.html (accessed on 11.02.2003).
99. Giannotta, G.; Morra, M.; Occhiello, E.; Garbassi, F.; Nicolais, L.; D'Amore, A. J. Colloid Interface Sci. 1992, *148*, 571.
100. Dahlbäck, L.M., Lundström T.S. Proceedings of ICCM-10, Whistler, B.C., 1995; III-293–III-300 pp.

101. Kissa, E. J. Text. Res. 1996, *66*, 660.
102. Hsieh, Y.-L.; Yu, B. Text. Res. J. 1992, *62*, 677.
103. Hsieh, Y.-L. Text. Res. J. 1994, *64*, 552.
104. Hsieh, Y.-L.; Thompson, J.; Miller, A. Text. Res. J. 1996, *66*, 456.
105. Labajos-Broncano, L.; González-Martin, M.L.; Bruque, J.M.; González-Garcia, C.M. J. Colloid Interface Sci. 2001, *233*, 356.
106. Siebold, A.; Nardin, M.; Schultz, J.; Walliser, A.; Oppliger, M. Colloids Surf. A 2000, *161*, 81.
107. Grundke, K.; Augsburg, A. J. Adhesion Sci. Technol. 2000, *14*, 765.
108. Etmanski, B.; Bledzki, A.K.; Fuhrmann, U. Kunststoffe 1994, *84*, 46.
109. Perwuelz, A.; Mondon, P.; Caze, C. Text. Res. J. 2000, *70*, 333.
110. Park, S.-J.; Jin, J.S. J. Polym. Sci. B, Polym. Phys. 2003, *41*, 55.
111. Grundke, K.; Boerner, M.; Jacobasch, H.-J. Colloids Surf. 1991, *58*, 47.
112. Grundke, K.; Bogumil, T.; Gietzelt, T.; Jacobasch, H.-J.; Kwok, D.Y.; Neumann, A.W. Progr. Colloid Polym. Sci. 1996, *101*, 58.
113. Tröger, J.; Lunkwitz, K.; Grundke, K.; Bürger, W. Colloids Surf. A 1998, *134*, 299.
114. Grundke, K.; Augsburg, A. J. Adhes. Sci. Technol. 2000, *14*, 765.
115. Giese, R.F.; Costanzo, P.M.; van Oss, C.J. Phys. Chem. Miner. 1991, *17*, 611.
116. Chibowski, E.; Holysz, L. Langmiur 1992, *8*, 710.
117. Washburn, E.W. Phys. Rev. 1921, *17*, 374.
118. Aranberri-Askargorta, I.; Lampke T.; Bismarck, A.; J. Colloid Interface Sci. 2003, *263*, 580.
119. Krüss Users Manual. K121 Contact Angle- and Adsorption Measuring System, Version 2.1, Part C, Krüss GmbH, 1996; 11 pp.
120. Fox, H.W.; Zisman, W.A. J. Colloid Sci. 1950, *5*, 514.
121. Chibowski, E.; Perea-Carpio, R. Adv. Colloid Interface Sci. 2002, *98*, 245.
122. Bubert, H.; Ai, X.; Haiber, S.; Heintze, M.; Brüser, V.; Pasch, E.; Brandl, W.; Marginean, G. Spectrochim. Acta, Part B: Atom. Spectrosc. 2002, *57*, 1601.
123. Ontiveros-Ortega, A.; Espinosa-Jiménez, M.; Chibowski, E.; González-Caballero, F. J. Colloid Interface Sci. 1998, *199*, 99.
124. Espinosa-Jiménez, M.; Giménez-Martin, E.; Ontiveros-Ortega, A. J. Colloid Interface Sci. 1998, *207*, 170.
125. Espinosa-Jiménez, M.; Ontiveros-Ortega, A.; Giménez-Martin, E. J. Colloid Interface Sci. 1997, *185*, 390.
126. Chibowski, E.; Espinosa-Jiménez, M.; Ontiveros-Ortega, A.; Giménez-Martin, E. Langmuir 1998, *14*, 5237.
127. Chibowski, E.; Ontiveros-Ortega, A.; Espinosa-Jiménez, M.; Perea-Carpio, R.; Holysz, L. J. Colloid Interface Sci. 2001, *235*, 283.
128. Chibowski, E.; González-Caballero, F. Langmuir 1993, *9*, 330.
129. Chibowski, E.; Bolivar, M.; González-Caballero, F. J. Colloid Interface Sci. 1992, *154*, 400.
130. Holysz, L.; Chibowski, E. Langmiur 1992, *8*, 717.
131. van Oss, C.J. Colloids Surf. A 1993, *78*, 1.
132. van Remoortere, P.; Joos, P. J. Colloid Interface Sci. 1991, *141*, 348.

133. Lee, L.-H. J. Adhesion 1998, *67*, 1.
134. Marmur, A. Adv. Colloid Interface Sci. 1992, *39*, 13.
135. Labajos-Broncano, L.; González-Martin, L.; Jańczuk, B.; Bruque, J.M.; González-Garcia, C.M. J. Colloid Interface Sci. 1999, *211*, 175.
136. Chibowski, E.; Holysz, L. J. Adhesion Sci. Technol. 1997, *11*, 1289.
137. Jones, W.C.; Porter, M.C. J. Colloid Interface Sci. 1967, *24*, 1.
138. Adam, N.K.; Jessop, G. J. Chem. Soc. 1865.
139. Grindstaff, T.H. Text. Res. J. 1969, *39*, 958.
140. Li, D.; Neumann, A.W. Surfactant Science Series. In *Applied Surface Thermodynamics*; Neumann, A.W. Spelt, J.K., Eds.; Marcel Dekker: New York, 1996; Vol. 63, 557 pp.
141. Li, S.K.; Smith, R.P.; Neumann, A.W. J. Adhesion 1984, *17*, 105.